Check for updates

Batteries & Supercaps

Review
doi.org/10.1002/batt.202400290

Chemistry Europe
European Chemical Societies Publishing

www.batteries-supercaps.org

Enhancing Voltage Output in Polyanion-Type Cathode Materials for Sodium Ion Batteries

Aifang Liu,[c] Suwan Lu,[b] and Xiaodong Wu*[a]

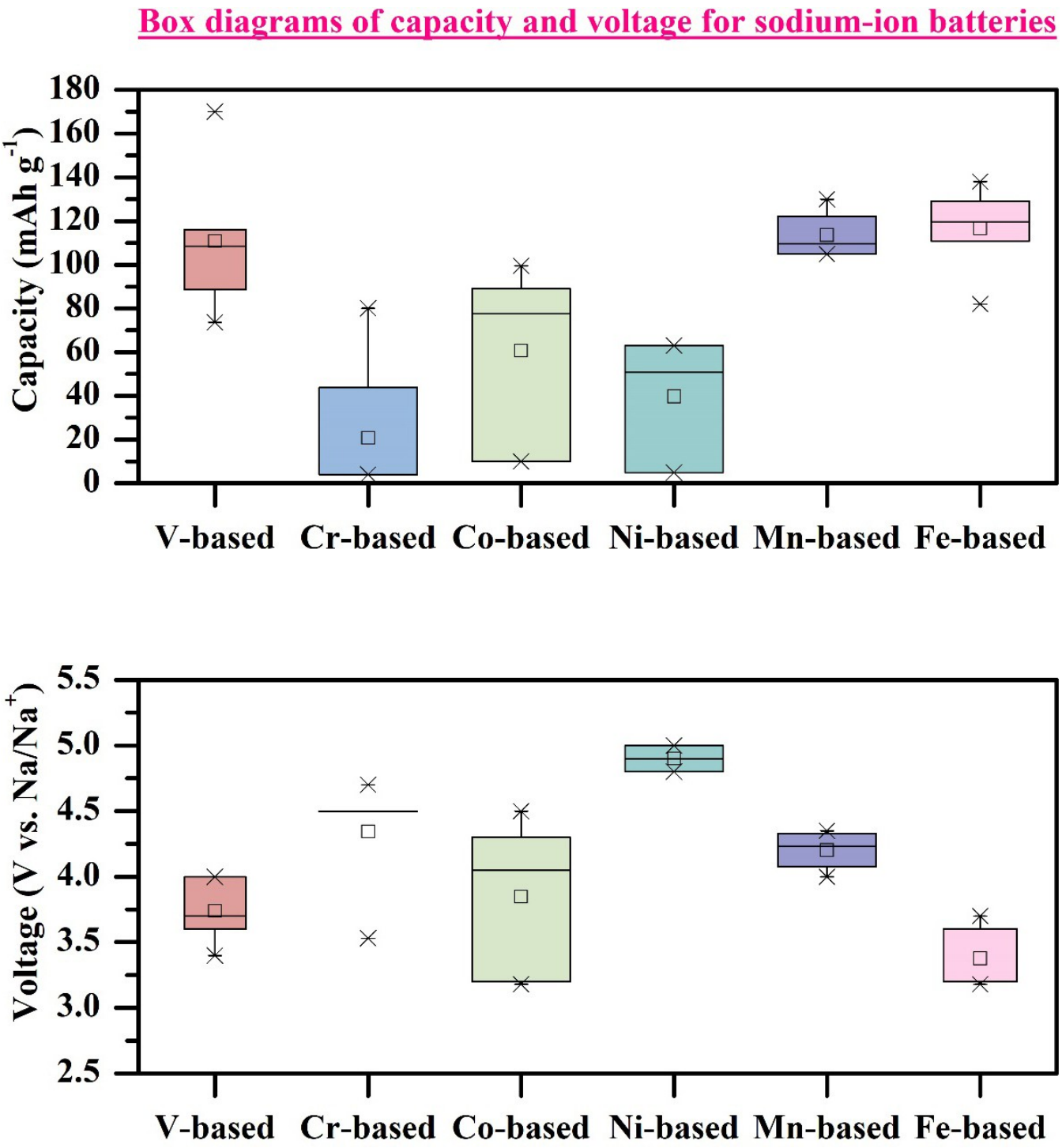

© 2024 Wiley-VCH GmbH

Sodium-ion batteries (SIBs) are promising in several aspects due to their many advantages over lithium-ion batteries. Among SIB's several outstanding attributes, its low cost, resource abundance, and potential safety make it suitable for large-scale energy storage systems (ESS). Among the potential cathode materials, poly-anionic cathode materials could be a better choice for their stability and safety in comparison to layered transition metal oxides and Prussian blue analogues (PBA). However, on the other hand, the conductivity as well as the available capacity of the polyanion compounds are still poor, which limits their applications; moreover, some polyanion cathode operate at low voltage, which reduces the energy density and raises the cost of the battery system. We here try to summarize the recent progress of polyanion compounds as cathode materials for SIB. These compounds are categorized based on the metal redox couple, including V-, Cr-, Mn-, Fe-, Co-, and Ni-polyanion compounds. Our attention is specifically drawn to properties such as reversible redox voltage, capacity, cycling stability, and sodium storage mechanisms. We also discuss the challenges and potential development strategies for the future.

1. Introduction

Sodium ion batteries (SIBs) have emerged as promising alternatives for large-scale energy storage due to the abundance of sodium resources and cost-effectiveness. Furthermore, SIBs have the potential to outperform lithium-ion batteries (LIBs) in certain aspects, such as operating at a wide temperature range[1] and exhibiting high-rate capability in specific cathode materials like $Na_3V_2(PO_4)_3$.[2] Although LIBs have made significant contributions to portable electronic devices, electric vehicles, and energy storage systems,[3] the shortage of Li resources and safety concerns highlight the need of further developing sodium ion batteries (SIBs).[4]

The low energy density of cathode materials is a challenging for developing sodium-ion batteries. Currently, three types of cathode materials are being explored, including layered metal oxides, Na-rich materials such as $Na_2M'O_3$ (M′ represents noble metals such as Ir, Ru, Sn, etc.), and polyanion-type materials. Undoubtedly, the shortcomings in low energy density can be addressed through higher output voltage and capacity.

Several drawbacks associated with the inherent structure of layered Na_xTMO_2 oxides ($0 < x \leq 1$, TM represents transitional metals such as Fe, Co, Mn, Ni, Cu, etc.) influence its cyclic stability,[5] including the structural evolution from Na^+/vacancy rearrangement, volume changes, severe phase transitions, particle fractures, and other issues that ultimately block the diffusion path. The structure is susceptible to slip gliding, with the edge-sharing MO_6 octahedral sheets stacked along the c-axis. Despite these shortcomings, they are still attractive due to their high energy density,[6] even though they exhibit low voltages not exceeding 3.5 V.[7] However, this limitation severely hinders their practical application. Another type of cathode material is the O_3-type high-Na-content layer oxide, stacked by alternative layers of Na and $[Na_{1/3}M_{2/3}]O_2$. It has been considered a promising candidate for practical application due to its inherent sufficient Na content. However, its capacity has been restrained by the low voltage threshold, considering the irreversible oxygen loss and the phase transition of the O_3-P_3 type.[8]

In contrast, polyanion-type materials possess advantages such as high operating potential, robust structural framework, and safety.[9] These robust structures are attributed to the corner or edge-sharing connections between MO_x [M = Fe, Mn, Co, V, Ti, Cr, etc.] and polyhedral and anion groups $(XO_4)_m^{n-}$ or $(X_mO_{3m+1})^{n-}$ [X denotes non-metal such as B, P, S, Si, etc.], which are beneficial for cycling stability.[10] The high output voltage can be adjusted by introducing polyanions with a strong ability to attract electrons from M–O bonds. This reduces obstacles in the metal redox reaction, by improving the redox potential. The electronegativity of the polyanion groups is ranked as $(SiO_4)^{4-} < (CO_3)^{2-} < (PO_4)^{3-} < F^- < (P_2O_7)^{4-} < (SO_4)^{2-}$,[10] so the polyanion cathode material structure can be varied by combining a metal active center with different polyanions, enabling improvements in high voltage for achieving high energy density. This paper classifies polyanion compounds into six types based on the metal redox center: V-based, Cr-based, Mn-based, Fe-based, Co-based, and Ni-based. The electrochemical performance, including indices such as operating voltage, discharge capacity, coulombic efficiency, and cycling stability, varies with the material structure,[11] cation doping,[12,13] transition-metal substitution[14,15] and defects engineering.[16]

1.1. The Structure of Polyanion Compounds

The formula for polyanion-type cathode materials can be expressed as $Na_xM_y(XO_4)_n$, where polyanion units can be $(XO_4)_n$ or their derivatives $(X_mO_{3m+1})_n$, with X representing elements such as S, P, Si, B, etc; and M representing a transition metal. Furthermore, there exist MO_x polyhedra with strong covalent bonds interconnected by oxygen atoms in the structure,[9,17]

[a] Prof. X. Wu
i-lab, Suzhou Institute of Nano-Tech and Nao-Bionics (SINANO), Chinese Academy of Sciences
398 Ruo shui Road, SEID, SIP, Suzhou, 215123, China
and
Nano Science and Technology Institute, University of Science and Technology of China, Hefei, 230026, China
E-mail: xdwu2011@sinano.ac.cn

[b] S. Lu
i-lab, Suzhou Institute of Nano-Tech and Nao-Bionics (SINANO), Chinese Academy of Sciences
398 Ruo shui Road, SEID, SIP, Suzhou, 215123, China
and
Nano Science and Technology Institute, University of Science and Technology of China, Hefei, 230026, China

[c] A. Liu
Department of Chemistry and Chemical Engineering
Taiyuan Institute of Technology
Xin Lan Road, Jian Cao Ping District, Taiyuan, 030008, China

© 2024 Wiley-VCH GmbH

25666223, 2024, 12, Downloaded from https://chemistry-europe.onlinelibrary.wiley.com/doi/10.1002/batt.202400290 by University of Ulsan, Wiley Online Library on [11/11/2025]. See the Terms and Conditions (https://onlinelibrary.wiley.com/terms-and-conditions) on Wiley Online Library for rules of use; OA articles are governed by the applicable Creative Commons License

contributing to a stable crystal lattice. However, these materials have low intrinsic electrical conductivity due to their unique structures. For instance, $NaFePO_4$ demonstrates two distinct phases, triphylite and maricite.[18] In the triphylite phase, one-dimensional sodium ions are constructed in a corner-sharing manner by sharing FeO_6 unit corners with PO_4, faciliating in Na^+ migration along the b-axis (Figure 1a). When the connection is by edge-sharing of adjacent FeO_6 units with PO_4, there is a lack of sodium diffusion channel, rendering it electrochemically inactive in the maricite phase (Figures 1b and c). Additionally, an amophous $NaFePO_4$ has been indentified (Figure 1d).[19] The polyanion-type compounds referenced in this paper are detailed in Table 1.

1.2. High Thermal Stability and Safety

In the polyanion crystal structure, oxygen atoms are linked into robust covalent bonds, allowing them to withstand thermal runway better than layered transition metal oxides. The robust 3D framework of polyanion compounds significantly decreases the structural variations during sodium ion insertion-desodiation, which contributes to the superior cycle stability, high safety and superior thermal abuse tolerance. These factors contribute to higher energy density and improved safety properties in large-scale applications.[17]

1.3. The Voltage of Polyanionic Compounds

The voltage linked to the formal charges of the central atoms in a system of polyanion-based cathode materials pertains to the

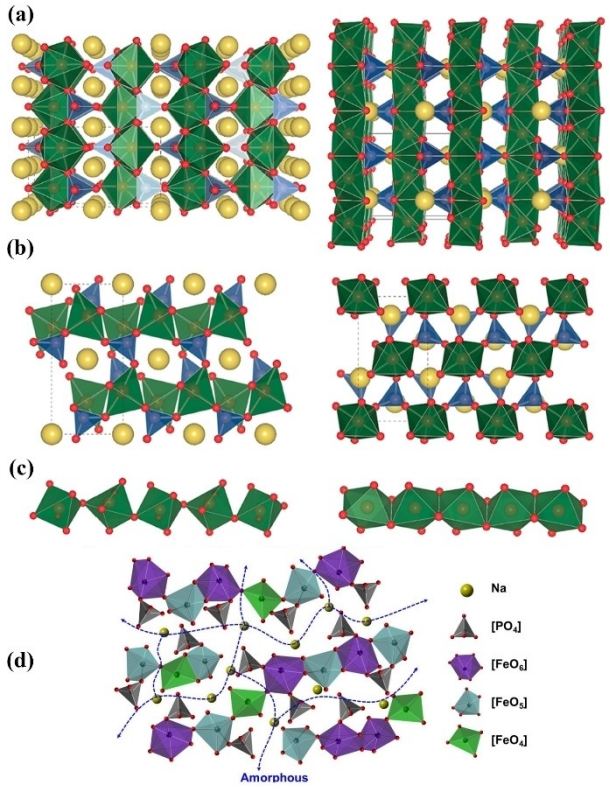

Figure 1. Crystal structure of (a) triphylite $NaFePO_4$ (left) and maricite $NaFePO_4$ (right). (b) FeO_6 octahedra (green), PO_4 tetrahedra (blue), and Na atoms (yellow). (c) Corner-sharing (left) and edge-sharing (right) coordination among neighbouring FeO_6 octahedra, respectively. (Reproduced from Ref. [18] Copyright (2013) with permission from American Chemical Society.) (d) Amorphous $NaFePO_4$. (Reproduced from Ref. [19] Copyright (2019) with permission from Elsevier.)

Xiaodong Wu is currently a Professor in Suzhou Institute of Nano-tech and Nano-Bionics (SINANO), Chinese Academy of Sciences (CAS), and also in the University of Science and Technology of China (USTC). He received his PhD degree from Institute of Physics, CAS. His research area focuses on electrode/electrolyte interface, solid state batteries, and also developing new type batteries.

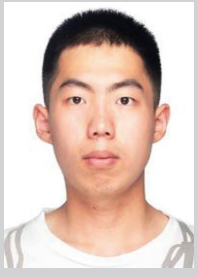

Suwan Lu obtained his bachelors in the major of Materials science and engineering from Sichuan University. He is currently a master in the materials and chemical industry at the Suzhou Institute of Nano-tech and Nano-bionics (Sinano), University of Science and Technology of China (USTC), under the supervision of Prof. Xiaodong Wu and associate Prof. Jingjing Xu. His research is focused on cathode design and electrolyte control of high specific energy sodium-based batteries and their applications in sustainable energy conversion and storage, encompassing lithium/sodium ions batteries, metal-sulfur/selenium batteries.

Aifang Liu received her PhD degree from the Department of Chemistry, Tongji University in 2011. She is now working as a lecturer at Taiyuan Institute of Technology. Her research is focused on the electrochemistry of rechargeable batteries and materials for new energy storage technology.

© 2024 Wiley-VCH GmbH

25666223, 2024, 12, Downloaded from https://chemistry-europe.onlinelibrary.wiley.com/doi/10.1002/batt.202400290 by University of Ulsan, Wiley Online Library on [11/11/2025]. See the Terms and Conditions (https://onlinelibrary.wiley.com/terms-and-conditions) on Wiley Online Library for rules of use; OA articles are governed by the applicable Creative Commons License

Review
doi.org/10.1002/batt.202400290
Chemistry Europe
European Chemical Societies Publishing

25666223, 2024, 12, Downloaded from https://chemistry-europe.onlinelibrary.wiley.com/doi/10.1002/batt.202400290 by University of Ulsan, Wiley Online Library on [11/11/2025]. See the Terms and Conditions (https://onlinelibrary.wiley.com/terms-and-conditions) on Wiley Online Library for rules of use; OA articles are governed by the applicable Creative Commons License

Table 1. Typical structure of polyanion-type cathode materials for SIBs reported in the reference.

Polyanion-type	Structure	Crystal	Space Group	Reference
$NaMPO_4$ (Fe, Co, Ni)	Olivine	Olivine	Pmnb	[20]
$NaMPO_4$ (Fe, Mn)	Maricite	Maricite	Pmna	[21]
$Na_3Fe_2(PO4)_3$	NASICON	Rhombohedral	C12c1	[22]
$Na_3Cr_2(PO_4)_3$	NASICON	Rhombohedral	R3c	[23]
$Na_3V_2(PO_4)_3$	NASICON	Rhombohedral	C2/c	[14]
$Na_2MP_2O_7$ (Fe, Mn)	/	Triclinic	P-1	[24]
$Na_2CoP_2O_7$	Layered	Orthorhombic	Pn21a	[18]
$Na_4M_3(PO_4)_2P_2O_7$(Fe, Ni, Co)	/	Orthorhombic	Pn21a	[10]
Na_2MPO_4F (Fe, Co)	/	Orthorhombic	Pn21a	[25]
Na_2MnSiO_4	/	Monoclinic	Pn	[26]
Na_2FeSiO_4	/	Triclinic	Fm3 m	[27]
Na_2CoSiO_4	/	monoclinic	Pn	[28]
$Na_2Fe_2(SO_4)_3$	/	Rhombohedral	R3c	[29]

concept of the inductive effect.[22] Figure 2 illustrates the operational voltages of polyanion-based cathode materials containing 3d transition metal with d-electron configurations used in sodium ion batteries.[30] Generally, transition metal ions M^{n+} with higher atomic numbers exhibit deeper valence levels due to a larger effective nuclear charge, leading to higher redox potentials for the $M^{(n+1)+}/M^{n+}$ pair.

In Figure 2, the operational voltage (average value) is observed to follow the sequence of Ni^{2+}/Ni^{3+} (4.5 V) > Co^{2+}/Co^{3+} (4.3 V) > V^{3+}/V^{4+} (3.8 V) > Mn^{2+}/Mn^{3+} (3.5 V) > Fe^{2+}/Fe^{3+} (3.0 V).[31] The potential difference is biggest for Ni^{2+}/Ni^{3+}, while the smallest difference is for Fe^{2+}/Fe^{3+}, compared to the baseline of Na^+/Na. When examining different frameworks with polyanion hosts, the redox energy for a fixed $M^{n+}/M^{(n+1)+}$ pair is usually the lowest in phosphates, while it is highest in mixed phosphates or pyrophosphates (shown in Figure 3). Among all polyanions, sulfate ions demonstrate the highest electronegativity and hence the strongest inductive effect, but they tend to decompose above 400 °C and are highly hygroscopic. Actually, certain redox couples vary significantly with different structures and polyanionic groups. The conclusions above could be explained according to the crystal-chemical theory proposed by Gutierrez,[32] which helps us fully understand the voltage trend of the $M^{n+}/M^{(n+1)+}$ pair in the polyanionic cathode by structural differences and the covalency of the polyanion. For example, shared edges in silicate structures increase energy of the redox couple, while polyhedral shared edges in phosphates decrease the redox potential of the couple. Although the theory was originally proposed based on the lithium-ion batteries, it is also available in sodium-ion batteries.

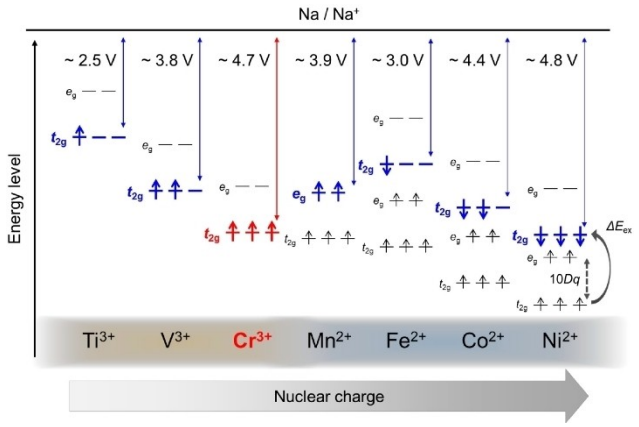

Figure 2. Schematic comparison of operating voltages and d-electron configurations for phosphate-based cathode materials containing 3d transition metal. $10D_q$ and E_{ex} indicate an octahedral crystal field splitting energy for 3d orbitals and exchange splitting energy, respectively. Reproduced from Ref. [30]. Published by MDPI. Copyright (2021) The Author(s).

2. Recent Progress of Polyanionic Materials

2.1. V-Base Redox

Among the V-based compounds considered for SIBs, those with the NASICON structure, such as $Na_3V_2(PO_4)_3$, stand out as promising candidates owing to the distinctive and robust three-dimensional framework that allows Na^+ rapid transport and high thermal stability. However, the space for improving the energy density is limited due to the low electrical conductivity of $Na_3V_2(PO_4)_3$. Techniques such as carbon coating,[33] heterogeneous element doping[34] and nano-structuring[35] are often employed as effective solutions to this issue. Simultaneously, substituting atoms at the Na,[36] V,[37] and P[38] sites within the structure has been found to enhance stability. Especially, the reversible reaction of the V^{4+}/V^{5+} couple in V-based NASICON

© 2024 Wiley-VCH GmbH

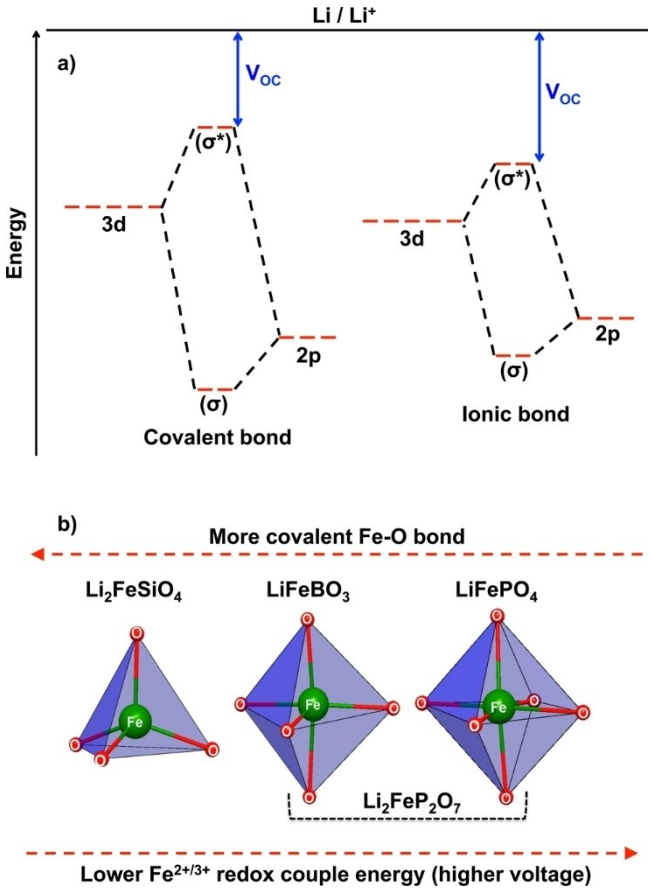

Figure 3. Schematic illustration of the effects of covalent and ionic M–O bond on the operating potential. (a) More covalent bond increases the repulsion between the bonding and antibonding orbitals. The increase in repulsion raises the antibonding orbitals closer to the Fermi level in lithium and lowers the voltage vs Li/Li^+ (b) Polyhedral in the borate, silicate, phosphate, and pyrophosphate compounds. As the coordination number decreases, the M–O bond becomes more covalent. (Reproduced from Ref. [32] Copyright (2013) with permission from American Chemical Society.)

materials can be significantly activated by partially substituting V with other transition metal ions such as Sc^{3+}, Mn^{2+} or Cr^{3+}. For example, the synthesized compound $Na_3V_{2-x}Sc_x(PO_4)_3$, substituted by Sc^{3+}, was studied by T. I. Perfilyenva et al.[39] As the substitution increased, the parameters and volume of the unit cell exhibited an increasing trend, while preserved the NASICON-type structure. The charging curves for all materials displayed two plateaus at around 3.5 V for the reaction V^{3+}/V^{4+} and at 4 V for the reaction V^{4+}/V^{5+} versus Na/Na^+ in sequential transitions. However, only the optimal $Na_3V_{1.5}Sc_{0.5}(PO_4)_3/C$ material showed reversibility at the high-voltage plateau upon discharge, enabling stable and reversible cycling between 1.0–4.5 V versus Na/Na^+ with a specific capacity exceeding 170 mAh g^{-1}. This capacity is equivalent to three Na^+ per formula unit during the de-intercalation process. Li et al[40] synthesized Mn/Si-codoped $Na_{3.5+x}V_{1.5}Mn_{0.5}(PO_4)_{3-x}(SiO_4)_x$ to enhance the reversible capacity and operating voltage. The optimized compound $Na_{3.55}Mn_{0.5}V_{1.5}(PO_4)_{2.95}(SiO_4)_{0.05}$ demonstrated remarkable improvements in cyclability and reversibility, with the slightly changed voltage plateau from 3.42 to 3.41 V. In contrast, for the $Na_3Mn_{0.5}V_{1.5}(PO_4)_3$ cathode, the voltage drops from 3.40 to 3.13 V due to severe voltage polarization and capacity degradation after 200 cycles at 2.5–4.2 V. Chen et al.[41] revealed that two redox reactions of V^{3+}/V^{4+} and V^{4+}/V^{5+} took place in Cr-doped $Na_3V_{1.5}Cr_{0.5}(PO_4)_3$, delivering a high capacity of 163.2 mAh g^{-1} at 1.0–4.2 V. Cai et al.[12] prepared a homovalent doped $Na_3V_2(PO_4)_2F_3/C$ material by meticulously designing the technological process to regulate the crystal structure and particle size in order to enhance the electrical conductivity. The synergistic effect of Cr^{3+} doping and carbon coating promoted rapid electron transport across $Na_3V_2(PO_4)_2F_3/C$ particles. These results corresponded to the smaller particle size and more uniform distribution (Figure 4b), compared to the agglomeration and irregular particle size of $Na_3V_2(PO_4)_2F_3/C$ (Figure 4a). XPS spectra of $NV_{1.98}Cr_{0.02}PF/C$ revealed peaks of Cr 2p at 586.5 eV and 578.38 eV (Figure 4c), indicating the insertion of Cr into the crystal structure. Additionally, the intensity of the absorption peak attributed to the vibration of P–O bond (Figure 4d), decreased with increasing Cr doping content, suggesting a decrease in bond distance and improved electrical conductivity. This indicates that Cr^{3+} doping enhances the electrical conductivity of the material. As a result, the optimal $Na_3V_{1.98}Cr_{0.02}(PO_4)_2F_3/C$ exhibited superior cycling performance, as depicted in Figure 4e. Furthermore, the structural stability of $Na_3V_{1.98}Cr_{0.02}(PO_4)_2F_3/C$ with retaining 93.62% of its capacity, compared to 82.64% of $Na_3V_2(PO_4)_2F_3/C$ after 200 cycles at 1 C, clearly indicates that the doped sample of $Na_3V_{1.98}Cr_{0.02}(PO_4)_2F_3/C$ exhibited much better electrochemical performance and more stable structural stability than the undoped samples of $Na_3V_2(PO_4)_3/C$. This improvement can be attributed to the shorten bond length of P–O and enhanced

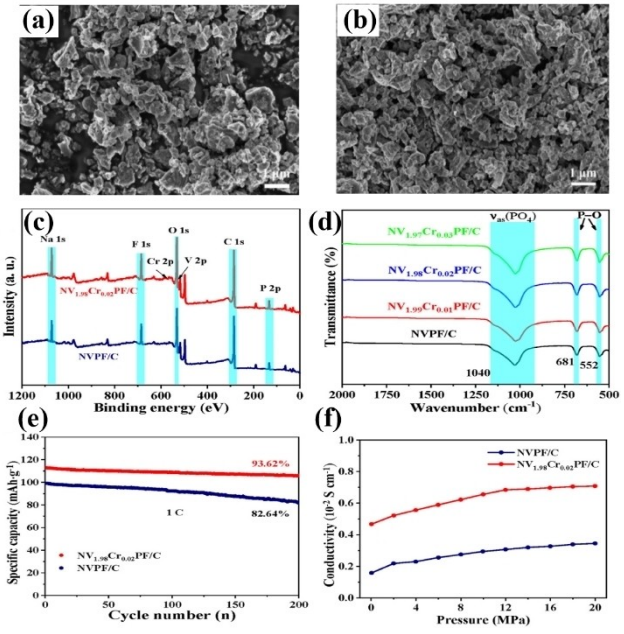

Figure 4. (a, b) SEM images of $Na_3V_2(PO_4)_2F_3$ and $NV_{1.98}Cr_{0.02}PF/C$, (c) XPS spectra of $Na_3V_2(PO_4)_2F_3$ and $NV_{1.98}Cr_{0.02}PF/C$, (d) FT-IR spectra of $NV_{2-x}Cr_xPF/C$. (e) Cycling performance at 1 C, (f) Electrical conductivity of $Na_3V_2(PO_4)_2F_3$ and $Na_3V_{1.98}Cr_{0.02}(PO_4)_2F_3/C$. (Reproduced from Ref. [12] Copyright (2023) with permission from Elsevier.)

© 2024 Wiley-VCH GmbH

25666223, 2024, 12, Downloaded from https://chemistry-europe.onlinelibrary.wiley.com/doi/10.1002/batt.202400290 by University of Ulsan, Wiley Online Library on [11/11/2025]. See the Terms and Conditions (https://onlinelibrary.wiley.com/terms-and-conditions) on Wiley Online Library for rules of use; OA articles are governed by the applicable Creative Commons License

electrical conductivity after Cr^{3+} doping, thereby facilitating Na^+ diffusion.

In order to extract the third Na^+ to increase the energy density, Chen et al.[42] designed the F-doped and V-vacancy $Na_3V_{1.98}(PO_4)_{3-x}F_{3x}$/C composites through a route available for scale-up production. The optimal sample was obtained when $x=0.1$ (F0.1-NV1.98 P/C), with a smaller particle size, uniform distribution (Figure 5a), and a clear crystal lattice coated by a thin carbon layer around 2 nm thick (Figure 5b). In the XPS spectra of V2p for the F0.1-NV1.98 P/C sample in a state of charging at 4.0 V, the peaks corresponding to V^{4+} are observed at 517.3 and 524.5 eV (Figure 5c), alongside additional peaks of V^{5+} at 518.1 and 525 eV (Figure 5d), which suggested that F-doped promotes the redox V^{4+}/V^{5+} reaction, leading to the extraction of the third Na. This observation is further supported by Figure 5e, the optimized F0.1-NV1.98 P/C composite, which delivers an initial charge capacity as high as 143.5 mAh g^{-1} and a discharge capacity of 116.9 mAh g^{-1} at 0.1 C. The V^{4+}/V^{5+} redox couple occurs at 4.0 V vs. Na/Na^+, and the reversibility is still considerable by changing the cycle rate (Figure 5f), which indicates shortened Na^+ diffusion pathways due to F-doping. These findings provide an accessible strategy and valuable insights for designing advanced F-doping and V-defect $Na_3V_{2-x}M_x(PO_4)_2F_3$/C cathode material for sodium-ion batteries.

Recently, high-Na-content materials have been explored as high-voltage (approximately 4.0 V average) cathodes for SIBs, offering capacities around 80 mAh g^{-1}. Kim et al.[43] demonstrated that $Na_7V_3(P_2O_7)_4$ achieved the highest operation average voltage at 4.13 V, attributed to each VO_6 octahedra sharing corners with P_2O_7 groups. The reversible insertion and extraction of Na^+ ions was up to three, but a higher voltage over 4.9 V is required to extract additional Na^+ ions. Based upon the $V^{3+}/^{4+}$ redox reaction, Lim et al.[44] reported a vanadium-based mixed phosphate $Na_7V_4(P_2O_7)PO_4$, which displays two peaks in the charging profile and only one peak in the reverse scanning. Moreover, the capacities may indicate the potential for four Na^+ transitions. This single-valued voltage behavior suggests the presence of an intermediate phase during iso-energetic structural rearrangements such as charge ordering and framework rotation, which could potentially lower reaction barriers, although such intermediate phases are not easy to tune. Fang et al.[45] confirmed that the compound $Na_7V_4(P_2O_7)PO_4$ demonstrates good cycling properties, retaining 81.4% capacity after 300 cycles at a 0.5 C rate, emphasizing the importance of achieving a pure phase for high-capacity electrode material. In another study by Masquelier et al.,[46] it was shown that Al substitution in the $Na_7V_4(P_2O_7)_4PO_4$ has an effect on the active part of the V^{4+}/V^{5+} redox couple during cycling, which could negatively impact electrochemical reversibility except for an additional capacity contribution.

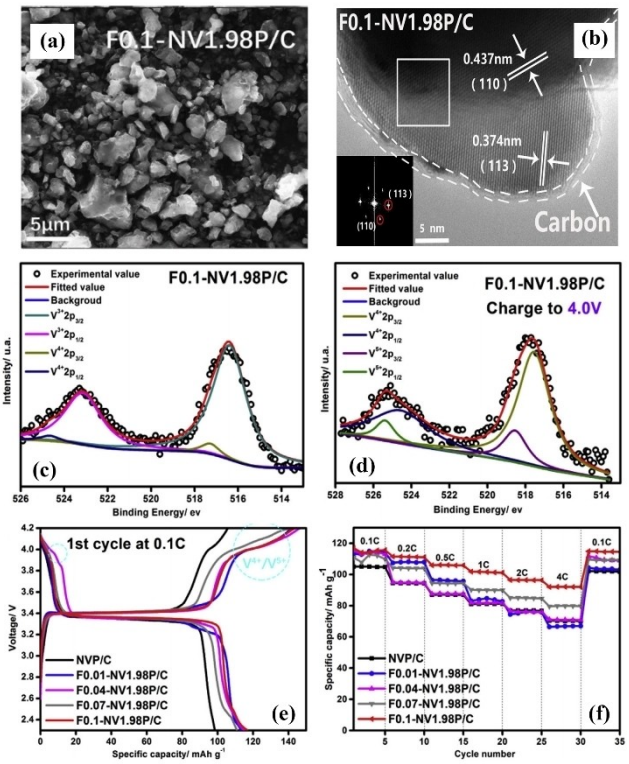

Figure 5. (a) SEM images of F0.1-NV1.98 P/C, (b) HRTEM image of F0.1-NV1.98 P/C sample. Inset graph is obtained from FFT, (c) XPS spectra of V2p for F0.1-NV1.98 P/C sample, (d) XPS spectra of V2p for F0.1-NV1.98 P/C sample charged at 4.0 V, (e) Initial galvanostatic voltage profiles at 0.1 C, (f) Capacity retention of discharge capacities at various current rates (0.1 C-4 C). (Reproduced from Ref. [42] Copyright (2023) with permission from Elsevier.)

As mentioned above, the energy density of the NASICON structure $Na_3V_2(PO_4)_3$ could be improved by incorporating heterogeneous ions into the crystal structure to induce intrinsic defects, thereby improving both electrical and ionic conductivity, consequently enhancing the output voltage and reversible capacity. It has been documented that the incorporation of ion dopants can either decrease the mean bond length or expand the unit cell volume related to the pathways for sodium diffusion. These dopants encompass both metal ions (such as Al, Mn, Sc and Cr) and non-metal ions (such as Cl and F). When compared to aliovalent metal ion doping, homovalent metal ion doping demonstrates superior electrochemical performance, including enhanced cycling performance and rate performance. Similar to Cr doping at the V site, the crystal structure of $Na_3V_2(PO_4)_2F_3$ produces substitution defects, leading to a rise in internal defect formation energy. This leads to improved electron transfer and ultimately enhances electronic conductivity. The high diffusion coefficient (1.40×10^{-14} $cm^2 s^{-1}$) of sodium ions for the $Na_3V_{1.98}Cr_{0.02}(PO_4)_2F_3$/C demonstrated improved conductivity. Additionally, it is necessary to activate the V^{4+}/V^{5+} redox couple through the realization of the third Na^+ in $Na_3V_2(PO_4)_3$ via trivalent ion doping in order to further increase the energy density. However, the durability of the cathode materials in a wide potential range is greatly influenced by the charge depth of vanadium (not to exceed 4.5 V). Deeper oxidation of vanadium cations results in significant distortion of the polyanionic framework, impeding reversible processes and causing rapid capacity degradation. As a conclusion, these results present V-based compounds as a potential cathode material for SIBs. Improvements on cycling stability and rate discharge capability are observed through carbon coating and element doping. The activation of the V^{4+}/V^{5+} redox couple from V-based polyanionic materials is promising to increase

© 2024 Wiley-VCH GmbH

25666223, 2024, 12, Downloaded from https://chemistry-europe.onlinelibrary.wiley.com/doi/10.1002/batt.202400290 by University of Ulsan, Wiley Online Library on [11/11/2025]. See the Terms and Conditions (https://onlinelibrary.wiley.com/terms-and-conditions) on Wiley Online Library for rules of use; OA articles are governed by the applicable Creative Commons License

25666223, 2024, 12, Downloaded from https://chemistry-europe.onlinelibrary.wiley.com/doi/10.1002/batt.202400290 by University of Ulsan, Wiley Online Library on [11/11/2025]. See the Terms and Conditions (https://onlinelibrary.wiley.com/terms-and-conditions) on Wiley Online Library for rules of use; OA articles are governed by the applicable Creative Commons License

energy density without inducing structural changes. However, given the toxicity and substantial cost of V, there has been a growing interest in partially or totally replacing it with more economical elements such Mn, Fe, Ni, Ti, Cr, and others, which has drawn more significant attention. These results in references are listed in Table 2.

2.2. Cr-Based Redox

Theoretical calculations by Hautier et al.[49] have suggested that the Cr^{4+}/Cr^{3+} redox couple is active. Subsequent work based on the theoretical conclusion by Herklotz et al.[50] confirmed this point in monoclinic $Li_3Cr_2(PO_4)_3$, but nearly delivered capacity when dealing with electrochemical activity. Expanding on this research, Kawai[23] introduced an exemplary NASICON-phase $Na_3Cr_2(PO_4)_3$, synthesized by a simple high-temperature calcination reaction, which demonstrates the activity of the redox of Cr^{4+}/Cr^{3+}. The cyclic voltammogram shows one cathodic peak and one anodic peak around 4.5 V within a potential window of 2.0–4.7 V at a 0.5 C rate, indicating the reversibility of the chromium redox. These observations not only highlight the potential to enhance the energy densities of SIBs but also signify the feasibility of stabilizing the high-valent state of chromium in these frameworks. Nevertheless, degradation in performance is observable due to overvoltage and voltage hysteresis. Excessive oxidation to Cr^{6+}, indicated by shifts in Cr K-edge X-ray Absorption Near Edge Structure (XANES) spectra upon charging, has been implicated in this phenomenon.

Remedial efforts by Kosuke Kawai[51] resulted in the stabilization of $Na_3Cr_2(PO_4)_3$ through partial substitution of Cr^{3+} with Ti^{4+}, aimed at mitigating structural distortions upon Na^+ uptake or removal due to its d^0 electronic configuration. However, negligible distortions nearly took place, contrasting with the initial expectation at the transition-metal sites, according to the analysis of the X-ray absorption spectroscopy (XAS) test results. This indicates that the effect of Ti^{4+} with d^0 configuration is irrelevant to the stability of the as-obtained $Na_2CrTi(PO_4)_3$ cathode material, which operates at 4.5 V vs. Na^+/Na with a retaining discharge capacity of 90% after the 50th cycle, indicating reversible phase evolution across a wide range of Na-composition and accompanying small lattice volume changes compared to other Ti-free analogues. Concurrent investigations by Zhang[52] on $Na_2TiCr(PO_4)_3$ emphasized a rhombohedral crystal structure (space group R3c) that hosts Cr^{3+} and Ti^{4+} ions with larger ionic radii, ensuring the stability of the Cr^{4+}/Cr^{3+} couple across an extended 2.5–5.0 V range for over 1000 cycles, unlike the NASICON-structured $Na_3Cr_2(PO_4)_3$, which showed a quick decline in capacity. In situ X-ray diffraction (XRD) analyses conducted during electrochemical cycling have uncovered distinct biphasic transitions. In contrast to the single-phase processes reported by Yamada et al.,[23] this two-phase reaction mechanism is primarily responsible for the small volume shrinkage of about 2.6% observed during the desodiation process. The optimal ratio of Ti:Cr in the stoichiometry of $Na_2TiCr(PO_4)_3$ was found to be most effective in sustaining the reversibility of the Cr^{4+}/Cr^{3+} redox reaction. Furthermore, the collaborative efforts of Ceder[53] with Cr–Mn synergies resulted in the $Na_4MnCr(PO_4)_3$ (NMCP) for SIBs, manifesting record NASICON-type cathode voltages averaging 3.59 V. Evaluations underscore robust coulombic efficiency (100%) and high Na reactivity at low voltages, despite capacity losses at higher voltages (4.35 to 4.5 V). Galvanostatic intermittent titration (GITT) has evidenced preferable Na diffusion in Na-deficient phases at elevated voltages, interplaying with compositional variances and high-voltage integrity. Moreover, temperature-dependent performances have been examined, with low-temperature operation notably paralleling ambient conditions, attributed to enhanced Na kinetics. X-ray absorption near-edge structure spectroscopy ascertains Mn and Cr activity at discrete voltage spectrum sectors (~3.9 V and ~4.3 V), coherent with predictive models. Yet, the reversibility of the Cr reaction diminishes in high voltage regions, suggesting structural deformations or potential material decomposition, which is related to Cr^{4+} mobility, considering migration barriers and the formation energy for Cr/Na anti-site defects are substantial. Given the low electronic conductivity found in NMCP materials, the approach by Zhang et al.[54] to incorporate a carbon matrix has significantly enhanced the electrochemical capabilities of $Na_4MnCr(PO_4)_3$, attributed to the outstanding Na^+ diffusion facilitating the process of the three-electron reaction process, resulting in a high energy density of 566 Wh kg^{-1}. These promising results have led to further research on the Na^+ storage mechanism to understand its differences from others. It has been determined that the low ionic-migration barrier is the main reason, a conclusion supported by the DFT computations and GITT measurements. Parallel to these developments, the work of Kosuke Kawai[55] showcases another leap in SIBs technology by achieving an operation voltage of 4.7 V vs. Na/Na^+ shown in Figures 6a and 6b, which is largely attributed to the high Cr^{4+}/Cr^{3+} redox potential in the $Na_{3-x}Cr_2(PO_4)_2F_3$ ($0 < x < 1$) system. The initial irreversible capacity is attributed to the anodic passivation reaction of the Al in the coin-cell parts, as well as other side reactions such as the oxidative decomposition of electrolyte and carbon additives, and the initial discharge capacity is 63.8 mA g^{-1} at 1 C between 2.7 V and 5.3 V (Fig-

Table 2. Electrochemical performance of V-based compounds.

V-based compounds	Voltage (V)	Rate (C)	Capacity (mAh g^{-1})	Cycles
Al doped $Na_3V_2(PO_4)_3$[47]	4.0	6 C	103 (0.5 C)	60
Sc doped $Na_3V_2(PO_4)_3$[39]	3.5/4.0	/	170 (1.0-4.5 V)	20
Mn/Si doped $Na_3V_2(PO_4)_3$[40]	3.6	10 C	116 (0.2 C)	200
Cr/F doped $Na_3V_2(PO_4)_3$[12]	3.7/4.2	20 C	114 (0.5 C)	200
Cl doped $Na_3V_2(PO_4)_3$[48]	3.4	30 C	88.54 (0.5 C)	5000
$Na_7V_4(P_2O_7)PO_4$[43]	3.88	0.5 C	73.6 (0.05 C)	1000

© 2024 Wiley-VCH GmbH

Review
doi.org/10.1002/batt.202400290
Chemistry Europe
European Chemical Societies Publishing

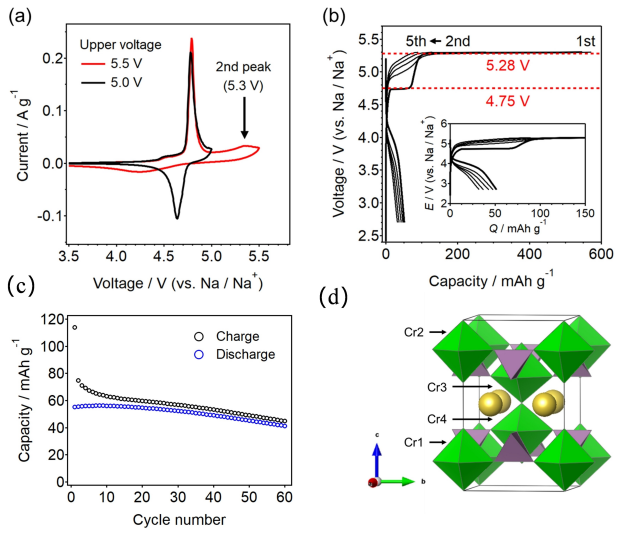

Figure 6. Performance of $Na_3Cr_2(PO_4)_2F_3$ electrode. (a) Cyclic voltammograms at 0.1 mV s^{-1} between 2.5 and 5.0 V (black line) or 5.5 V (red line), (b) Charge/discharge profiles between 2.7 and 5.3 V at 1 C (1 C = 63.8 mA g^{-1}), (c) Cycling performance of $Na_3Cr_2(PO_4)_2F_3$ electrode in Na half-cell at a rate of 0.1 C between 2.7 and 5.0 V vs. Na/Na^+. (d) Model structure for charge-separated Cr atoms in $Na_3Cr_2(PO_4)_2F_3$ using the background function of Legendre polynomials with Sonneveld-Visser method. (Reproduced from Ref. [55] Copyright (2021) with permission from American Chemical Society.)

ure 6c). figure 6d shows the charge Cr separated in the model structure based on the Sonneveld-Visser method. The study indicates that the strategic selection of materials, especially those that exploit the redox potential of early transition metals like chromium, can lead to high-voltage electrode materials without the need for late transition metals that were traditionally utilized for achieving potentials over 4.2 V. This illustrates a promising avenue for further development of high-voltage SIBs, unveiling a new paradigm in the pursuit of efficient and cost-effective energy storage technologies. The electrochemical performance of Cr-based compounds is listed in Table 3 below.

In conclusion, the cyclability of the Cr^{4+}/Cr^{3+} redox couple has been improved in the NASICON-type phosphate $Na_2TiCr(PO_4)_3$ through Ti^{4+} substitution, making it a promising high-voltage cathode material for sodium-ion batteries. Despite Ti with d^0 electronic configuration, which does not directly influence the local environment of the transitional metal, it plays a crucial role in stabilizing the redox of Cr^{4+}/Cr^{3+} in the high-voltage range, particularly when the optimal ratio of Ti and Cr is achieved. The enhanced cycling stability is attributed to a small biphasic miscibility gap during phase evolution across the wide Na-composition range, resulting in a small lattice volume change during the de-intercalation process. While redox couples like Co^{3+}/Co^{2+} or Ni^{3+}/Ni^{2+} demonstrate high voltage operation within polyanionic frameworks, the abundance of Cr^{4+}/Cr^{3+} presents a compelling option for designing high-voltage cathode materials. Notably, $Na_{3-x}Cr_2(PO_4)_2F_3$ compounds have been identified to operate at an extraordinary high potential of 4.7 V versus Na/Na^+, surpassing many cathode materials for LIBs.[55] This suggests potential for cost-effective, high-voltage alternatives in future material development within polyanion compounds. However, challenges persist regarding cycling stability in practical applications, particularly in high-voltage regions. Additionally, the energy density of the Cr^{4+}/Cr^{3+} redox couple in the reported NASICON-type compounds remains relatively low, even without considering the toxicity of chromium. Addressing these issues will be crucial for the future development and commercialization of Cr^{4+}/Cr^{3+} based-cathode materials.

Table 3. Electrochemical performance of Cr-based compounds.

Cr-based compounds	Voltage (V)	Rate (C)	Capacity (mAh g^{-1})	Cycles
[23]$Na_3Cr_2(PO_4)_3$	4.5	1 C	80 (1.0 C, 2.5–4.7 V)	20
[51]$Na_2CrTi(PO_4)_3$	4.5	/	43.7 (0.05 C, 2.5–4.7 V)	50
[56]$Na_2CrTi(PO_4)_3$	4.5	5 C	49.9 (0.3 C, 2.5–4.7 V)	1000
[54]$Na_4MnCr(PO_4)_3$	3.53	5 C	160 (0.05 C,1.2–4.6 V)	50
[55]$Na_3Cr_2(PO_4)_2F_3$	4.7	1 C	60 (1.0 C, 2.7–5.0 V)	60

2.3. Co-Based Redox

The output voltage based on the Co^{2+}/Co^{3+} redox couple can be arranged in the order of PO_4 (4.19 V) < PO_4F (4.3 V) ≈ P_2O_7 (4.3 V) < $(PO_4)_2P_2O_7$ (4.4 V).[31] In the case of olivine $NaCoPO_4$, synthesizing single-phase $NaCoPO_4$ is challenging due to the close enthalpies of formation. The electrochemical performance of polyanionic cathode materials is related to the conditions of synthesis, nonstoichiometric factors, and the control of polymorphism. In 2017, Arturo et al.[57] utilized microwave radiation to rapidly synthesize a $NaCoPO_4$ (NCP) polymorph at a low temperature of 200 °C. Moreover, the electrochemical activity was evaluated by the characteristic means, including ex-situ XRD and XANES. More recently, Aditi Chiring et al.[58] disclosed that $NaCoPO_4$ uniquely crystallizes into four different structures, which are influenced by the calcination temperature. All-phase $NaCoPO_4$ exhibited limited charge and discharge capacities due to a deficiency in sodium ion diffusion channels, as indicated by the electrochemical properties. The lower voltage of 3.0 V can be explained by the substantial Co–O covalency due to the Co center's fourfold coordination in CoO_4 tetrahedra. It is worth noting that the slight changes in intercalation voltages are linked to the presence of Na^+ in various surroundings.

For high voltage $Na_2CoP_2O_7$ cathodes, three types of phases have been identified as a tetragonal phase, a triclinic phase known as the red phase, and an orthorhombic phase known as blue phase. The "red" phase is constructed from corner-shared pyrophosphate (P_2O_7) groups and Co–O, while the "blue" phase is characterized by alternating Na layers and Co–P–O layers.

© 2024 Wiley-VCH GmbH

25666223, 2024, 12, Downloaded from https://chemistry-europe.onlinelibrary.wiley.com/doi/10.1002/batt.202400290 by University of Ulsan, Wiley Online Library on [11/11/2025]. See the Terms and Conditions (https://onlinelibrary.wiley.com/terms-and-conditions) on Wiley Online Library for rules of use; OA articles are governed by the applicable Creative Commons License

Among these, the red phase stands out for its superior electrochemical performance. Choi's group[59] has unveiled that the ionic size and crystal field stabilization contribute to the relative stability of different polymorphs, leading to intensive studies on metal substitution within the crystal lattice. Their findings revealed that $Na_2Co_{1-x}M_xP_2O_7$ polymorphs substituted by Ca, Ni, or Mn display increased voltage up to 4.3 V, and enhanced capacities compared to the $Na_2CoP_2O_7$ blue phase. Additionally, sodium deficiencies are favorable for inducing the red phase; increasing Na vacancies stabilizes the rose phase.[60] In recent years, mixed $[PO_4]$ and $[P_2O_7]$ group compounds, $Na_4M_3(PO_4)_2P_2O_7$ have emerged as leading cathode candidates for practical applications. The high average voltage at around 4.5 V based on Co^{2+}/Co^{3+} redox in $Na_4Co_3(PO_4)_2P_2O_7$ was initially reported by Nose et al.[61] Cabanas and his colleagues investigated the reaction mechanism and structural evolution during electrochemical cycling of the $Na_4Co_3(PO_4)_2P_2O_7$ by utilizing operando XRD coupled with electrochemical impedance spectroscopy (EIS).[62] Unlike the phosphate framework, the pyrophosphate structures 3D channels that accommodate various Na^+ sites, leading to multistep deintercalation during the ion transition, which indicated a complex mechanism. Density functional theory (DFT) calculations have shown that, despite being isostructural, Fe-, Mn-, and Ni-based materials undergo distinct reaction mechanisms. Its crystal structure facilitates 3D tunnels along the primary crystallographic axes with four symmetrically distinct Na sites. The material exhibited greater stability, reversibility, and higher capacity compared to its isostructural Fe- and Mn-based analogs, which experience a single-phase solid-solution reaction. While $Na_4Co_3(PO_4)_2P_2O_7$ exhibits multiple redox plateaus and biphasic region formation, as evidenced by the corresponding operando XRD pattern during charge and discharge processes. These phenomena might reflect specific Na^+/Vacancy ordering schemes.[63] The evolution of all reduced cell parameters in $Na_4Co_3(PO_4)_2P_2O_7$ differs from that of other isostructural compounds. The structural environment near Na vacancies has changed, leading to alterations in the $[CoO_6]$ octahedra, causing numerous phase transitions and conferring high structural stability. Liu et al.[13] reported Al-doped high-voltage cathode $Na_4Co_3(PO_4)_2P_2O_7$ (NCPP) exhibiting exceptional long-term cycling performance. The structural stability of the cathode material was enhanced by the substitution Co^{2+} by Al^{3+}, which improved electrical conductivity by creating vacancies. This substitution also helped prevent crystal collapse and led to changes in lattice parameters. The Rietveld refinement results suggest that Co1 sites were partially occupied by doping Al, resulting in the formation of AlO_6 octahedra. In addition, electrolyte stability is an important factor. Zeng et al.[64] studied the stability of the $Na_4Co_3(PO_4)_2P_2O_7$ in combination with a SIB electrolyte of low concentration as designed by Guan et al.,[65] characterized by low cost, non-flammability, and enhanced oxidation stability. The introduction of the novel electrolyte has significantly improved the performance of sodium-ion batteries using NASICION-type cathode materials (NCPP). The special Na^+ solvation sheath structure and anion distribution greatly improve the electrolyte's oxidation stability. The Na//NCPP cells demonstrated impressive results, retaining 70.58% of their capacity and achieving an average coulombic efficiency (CE) of 98.74%. The enhanced oxidation stability of the electrolyte during high-voltage cycling can be attributable to a dense and thin film formed between the cathode and electrolyte phases, which enhances the stability of the interface between the electrolyte and the cathode material. Notably, the absence of surface cracking on the NCPP cycled with this new electrolyte contrasts with the significant narrow cracks observed on the cathode cycled with the traditional electrolyte. As a result, the cells maintain robust cycle stability even when charged to a high voltage of up to 4.7 V. In another study by A. Chari et al.,[66] $Na_3ZrCo(PO_4)_3$ cathode material was obtained using a sol-gel method, yielding promising results. The discharge plateau occurred at a high voltage of 4.05 V, and the specific capacity was 85 mAh g^{-1} observed in the discharging curve at 0.1 C within the voltage window of 2.0–4.4 V (Figure 7c), releasing approximately 80% of the theoretical capacity of 106 mAh g^{-1}, with a capacity retention of 83.5%. Rate capability performance showed that when the rate returned to 0.1 C, almost all of the capacity was reversible after 50 cycles (Figure 7d). These findings correlate with slight variations in lattice parameters and a modest volume change of 3.8%, which are attributed to Zr^{4+} keeping the same valence state so as to stabilize the material structure, for the Co/ZrO_6 octahedral sharing their corners (Figure 7a). Furthermore, the improved conductivity by coating crystalline graphite (Figure 7b) on the surface of the $Na_3ZrCo(PO_4)_3$ cathode material also enhanced the electrochemical performance. K. Kubota et al.[67] reported the synthesis of Na_2CoPO_4F at 650 °C, modified with ascorbic acid as a carbon source, which exhibits the highest operating voltage of 4.3 V vs. Na^+/Na among the Na_2MePO_4F series, where Me can be Fe, Co, or Mn, thus possessing an estimated energy density reaching

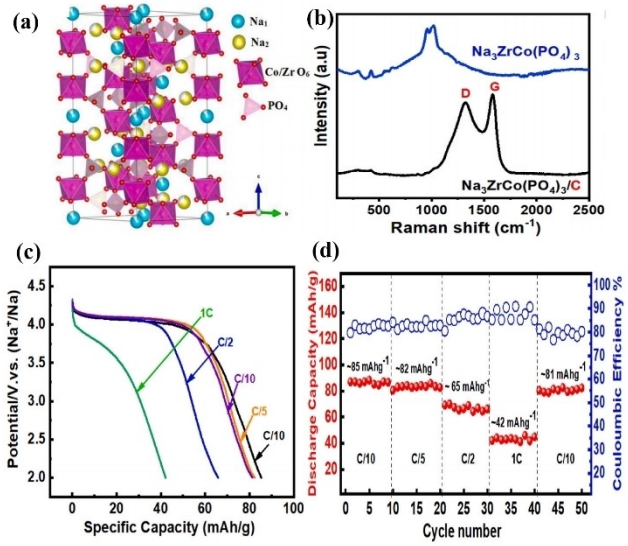

Figure 7. (a) Crystal structure of Na3CoZr(PO4)3, (b) Raman spectra of the uncoated and coated $Na_3CoZr(PO_4)_3$ samples; (c) Discharge curves of the $Na_3CoZr(PO_4)_3$/ C sample at different rate in voltage range of 2.0–4.4 V, (d) Rate capability of the $Na_3CoZr(PO_4)_3$/C electrode. (Reproduced from Ref. [66] Copyright (2022) with permission from Elsevier B.V.

© 2024 Wiley-VCH GmbH

25666223, 2024, 12, Downloaded from https://chemistry-europe.onlinelibrary.wiley.com/doi/10.1002/batt.202400290 by University of Ulsan, Wiley Online Library on [11/11/2025]. See the Terms and Conditions (https://onlinelibrary.wiley.com/terms-and-conditions) on Wiley Online Library for rules of use; OA articles are governed by the applicable Creative Commons License

25666223, 2024, 12, Downloaded from https://chemistry-europe.onlinelibrary.wiley.com/doi/10.1002/batt.202400290 by University of Ulsan, Wiley Online Library on [11/11/2025]. See the Terms and Conditions (https://onlinelibrary.wiley.com/terms-and-conditions) on Wiley Online Library for rules of use; OA articles are governed by the applicable Creative Commons License

407 Wh kg^{-1} based on metallic sodium as a promising cathode. These studies highlight the significant potential of these cathode materials for high-performance sodium-ion batteries, offering enhanced energy density and stable cycling performance. The electrochemical performance of Co-based compounds is listed in Table 4.

As a conclusion, the Co^{2+}/Co^{3+} redox operates above 4.0 V when extracting from the polyanion-based hosts, making it promising for high-voltage cathode materials. Phosphate and pyrophosphate compound materials have relatively low activity due to the strong Co–O bonds. By mixing [PO_4] and [P_2O_7] group to form 3D tunnels facilitating the Na^+ reversibility surpassing isostructural Fe- and Mn-based analogs, the $Na_4Co_3(PO_4)_2P_2O_7$ exhibits multiple redox plateaus and biphasic region formation, which is different from the single-phase solid-solution reaction over the full voltage range compared with the isostructural Fe- and Ni-based compounds experience. The better electrochemical performance and the oxidation stability are achieved even undergoing through high voltage operation. However, due to the scarcity and high cost of cobalt, research efforts focus on regulating cobalt amounts and developing cost-effective recycling processes.

2.4. Ni-Based Redox

The olivine $NaNiPO_4$ has been calculated theoretically to have at output voltage of 4.58 V.[71] However, the commonly obtained $NaMPO_4$ phase under standard synthesis conditions is the maricite phase, which is electrochemically inactive, unlike $LiMPO_4$ compounds. Recognizing the potential of combining different polyanionic groups to enhance ion diffusion and voltage profiles in SIBs during the sodiation/desodiation process, Passerini et al.[63] first demonstrated the activity of the Ni^{2+}/Ni^{3+} redox in $Na_4Ni_3(PO_4)_2P_2O_7$. This compound adopts an orthorhombic structure (Pn21a), which shares similarities with the structure of $Na_4Co_3(PO_4)_2(P_2O_7)$. Structural analysis indicated that Na ions occupy four distinct sites within the large channels formed by the P_2O_7 dimers. The presence of mixed polyanions may stabilize the charged Ni species and improve Na^+ ion diffusion and reversibility, compared to $NaNiPO_4$ and $Na_2NiP_2O_7$. Regarding electrochemical processes using ionic liquid-based electrolytes with expanded electrochemical stability windows, it has been noted that anodic peaks occur at 4.61 V, 4.67 V, and 5.5 V, while two reversible cathodic peaks are observed at 4.58 V and 4.92 V on the differential capacity (dQ/dV) curves. These peaks correspond to about half of the theoretical capacity of 127 mAh g^{-1}. No phase transitions or irreversible structural reorganizations were detected by ex situ XRD pattern analysis between 3.1 V and 5.0 V. The insertion of 1.3 Na, which is less than the extraction of 2.7 Na equivalents, suggests that the re-insertion path is obstructed due to the collapse of the [$Ni_3P_2O_{13}$] layers. The incorporation of phosphate and pyrophosphate units into a polyanionic structure enables the reversible uptake and release of approximately 1.3 Na^+ ions, operating at an average potential of approximately 4.8 V. However, Ni in the $Na_2NiP_2O_7$/C electrode does not exhibit activity.

In the realm of electrochemical studies, P. Ramesh Kumar[72] delved into the investigation the electrochemical properties of a carbon composite $Na_4Ni_3(PO_4)_2P_2O_7$, utilizing a high-voltage dimethyl carbonate-based electrolyte. The prepared particle size was about 600 nm (Figure 8a) with a large pore structure due to the surface carbon coating (Figure 8b). This structure was beneficial for improving electronic conductivity. Notably, the CV curve depicted two distinct voltage plateaus around 4.9 V and 4.6 V (figure 8c), corresponding to the four sodium crystallographic sites in the crystal structure. To exclude the influence of electrolyte decomposition, the cells underwent capacity-limited cycling within a voltage range of 1.7–5.1 V to intercalate/de-intercalate only 1.3 Na^+ (Figure 8d), avoiding structural deformation that occurs when up to 3 Na^+ are

Table 4. Electrochemical performance of Co-based compounds.

Co-based compounds	Voltage (V)	Rate (C)	Capacity (mAh g^{-1})	Cycles
[58]$NaCoPO_4$	/	C/25	10 (C/25, 2.5–4.8 V)	3
[68]$Na_4Mn_2Co(PO_4)_2P_2O_7$	3.86	0.2	96.1 (0.2 C, 1.7–4.6 V)	150
[69]$Na_4Co_3(PO_4)_2P_2O_7$	4.5	0.1	70 (0.1 C, 2.7-4.8 V)	100
[13]$Na_{3.85}Co_{2.85}Al_{0.15}(PO_4)_2P_2O_7$	2.88/3.18	50	99.5 (0.5 C,1.5–4.8 V)	900
[70]$Na_3ZrCo(PO_4)_3$	4.05	2	85 (0.1 C, 2.0–4.8 V)	50
[67]Na_2CoPO_4F	4.3	0.1	89 (0.1 C, 2.0–5.0 V)	5

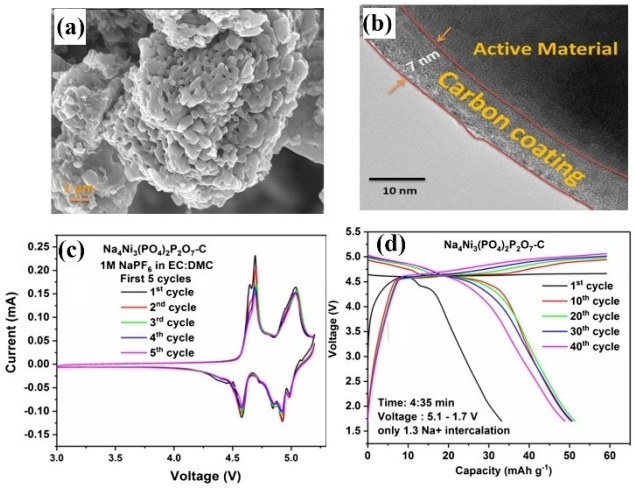

Figure 8. (a) SEM images of $Na_4Ni_3(PO_4)_2P_2O_7$-C, (b) TEM images of $Na_4Ni_3(PO_4)_2P_2O_7$-C, (c) The first five CV cycles for $Na_4Ni_3(PO_4)_2P_2O_7$-C and composites in 1 M $NaPF_6$ in EC: DMC electrolyte, (d) Charge-discharge curves within the voltage range of 1.7–5.1 V (Reproduced from Ref. [71] Copyright (2022) with permission from Springer).

© 2024 Wiley-VCH GmbH

involved. The discharge curve displayed a consistent capacity of 51 mAh g^{-1} at 0.1 C at the 40th cycle (Figure 8d). This indicates that the structural stability of the high-voltage cathode relies on the level of sodium participation in the transition during the initial cycles. Stability in cycling was achieved when sodium intercalation/de-intercalation was restricted to 1.3 Na^+ to ensure electrolyte stability.

In a prior study by Kundu et al.,[73] a single crystal of $Na_4NiP_2O_7F_2$ was synthesized and subjected to atomistic-scale calculations. Structural characteristic analyses confirmed the existence of a three-dimension open framework structure facilitating Na^+ ion migration by lowering transfer energy in all three directions, along with demonstrating thermal stability from 20 to 800 °C, even in an ambient atmosphere. However, extraction took place at a voltage of about 5–5.2 V with only 0.35 Na^+, provided the electrolyte remained stable in the absence of the cathode. The integration of highly electronegative F^- groups alongside P–O moieties enhanced the redox capability of the Ni^{2+}/Ni^{4+} couple within a high-charge region between 4.7 V and 5.2 V.[32] The electrochemical performance of Ni-based compounds is listed in Table 5.

Due to their low electronic conductivity, leading to limited alkali ion diffusion, Ni-based polyanionic materials have been regarded as inactive cathode materials in both lithium and sodium systems. Although the use of mixed polyanion can improve Na ion diffusion and carbon coating can enhance electronic conductivity, only 1.3 Na^+ can be extracted during the electrochemical process, compared to the four Na^+ present in the compound. In conclusion, the choice of transition metal significantly impacts the operating potential. Both Co-based and Ni-based cathode materials are recognized as 4 V-class cathodes. For example, $Na_{2-2x}Co_{1+x}P_2O_7$ with the output voltage at 4.0 V, $Na_4Co_3(PO_4)_2P_2O_7$ at 4.4 V, and $Na_4Ni_3(PO_4)_2P_2O_7$ at 4.8 V vs. Na/Na^+. Although alternatives such as $Na_3V_2(PO_4)_2F_{3-x}O_x$ and $Na_7V_3(P_2O_7)_4$ containing vanadium show promise, the utilization of V, Co, or Ni as the metal redox center poses challenges in battery production due to their cost and toxicity. The high oxidative properties of Co and Ni redox couples exhibit activity at 4.5 V but are apt to induce side reactions unless careful design strategies are implemented for both the electrolyte and electrode composite.

Table 5. Electrochemical performance of Ni-based compounds.

Ni-based compounds	Voltage (V)	Rate (C)	Capacity (mAh g^{-1})	Cycles
[72]$Na_4Ni_3(PO_4)_2P_2O_7$/C	4.8	0.01	63 (0.01 C, 3.0–5.1 V)	/
[63]$Na_4Ni_3(PO_4)_2P_2O_7$	4.9/4.6	0.1	51 (0.1 C, 1.7-5.1 V)	40
[73]$Na_4NiP_2O_7F_2$	>5	0.03	5 (0.03 C, 3.0–5.5 V)	/

2.5. Mn-Based Redox

Most polyanion hosts initially only utilized the Mn^{3+}/Mn^{2+} redox couple.[72,73] However, Mn-based NASICON-type $Na_xMnM(PO_4)_3$ materials have drawn extensive attention due to their ability to activate both Mn^{4+}/Mn^{3+} and Mn^{3+}/Mn^{2+} redox processes. Nonetheless, the presence of John-Teller distortions in Mn^{3+} sites has led to performance issues. To address this challenge, the incorporation of additional transitional metals into the NASICON structure offers numerous advantages. For example, $Na_3MnTi(PO_4)_3$ enables stable long-term cycling while facilitating both Mn^{4+}/Mn^{3+} and Mn^{3+}/Mn^{2+} redox reactions. However, it exhibits instability at high voltages around 4.0 V during cycling.[76] Gao et al.[77] synthesized NASICON-structured $Na_3MnZr(PO_4)_3$ through a sol-gel method, demonstrating a higher 4.0 V discharge voltage for Mn^{4+}/Mn^{3+} redox compared to other manganese phosphates, such as $Na_2MnP_2O_7$ (3.6 V) and $Na_4Mn_3(PO_4)_2P_2O_7$ (3.8 V) for sodium batteries.[78] Additionally, the issue of the Jahn-Teller effect of Mn^{3+} was relieved by Zr-doppping, balancing the strain of the distortion with a different local environment. This led to improved reversibility, as evidenced by a higher initial coulombic efficiency of 87% than that of other manganese phosphate.[77,78] Moreover, its capacity retention was 91% of its initial capacity after cycling 500 times at 0.5 C, with a minimal volume change of about 5% due to the distorted octahedral sites of Mn^{3+} being affected by various environments rather than Jahn-Teller effects, and the stable intermediate-phase $Na_2MnZr(PO_4)_3$ during Na^+ exchange. Contrary to previous theoretical predictions that focused on NASICON-structured with a single octahedral-site transition-metal cation, $Na_3MnZr(PO_4)_3$ contains two distinct cations, enhancing its structure further. Zhang et al.[80] reported a novel NASICON-type $Na_4MnCr(PO_4)_3$ material with uniform particle size ranging from 0.5–1 μm (Figure 9a), a thin amorphous carbon coating with some degree of graphitization (Figure 9b), and well-defined crystallization with a rhombohedral structure characterized by a selected area electron diffraction (SAED) pattern (Figure 9c). The electrochemical performance exhibited a highly reversible two-step reaction at potentials of 4.15 and 3.52 V versus Na^+/Na (Figure 9f), corresponding to Mn^{4+}/Mn^{3+} and Mn^{3+}/Mn^{2+} redox reactions. Upon charging to 3.9 V, the peak of Mn $2p_{3/2}$ suggested the appearance of Mn^{3+} (Figure 9d). When further charged to 4.3 V, the binding energy of Mn $2p_{3/2}$ shifted to 642.10 eV, implying the formation of Mn^{4+}. In contrast, the binding energies of Cr 2p kept consistent throughout the entire charging process (Figure 9e). The energy density, calculated by multiplying the capacity by the voltage, equals an energy density of over 500 Wh kg^{-1}, surpassing other works. The presence of Cr^{3+} helps maintain less than 50% of Mn^{3+} in transitional metal sites, thereby suppressing Jahn-Teller distortions and improving the structural stability during repeated de/intercalation of Na^+ ions. The robust NASICON framework of $Na_4MnCr(PO_4)_3$ also lowers the diffusion energy barrier, contributing to its superior electrochemical performance. The unique process of two-phase formation and the creation of a solid solution interphase aid in releasing the strain during the Na^+ shuttle within the crystal structure. Wang

© 2024 Wiley-VCH GmbH

25666223, 2024, 12, Downloaded from https://chemistry-europe.onlinelibrary.wiley.com/doi/10.1002/batt.202400290 by University of Ulsan, Wiley Online Library on [11/11/2025]. See the Terms and Conditions (https://onlinelibrary.wiley.com/terms-and-conditions) on Wiley Online Library for rules of use; OA articles are governed by the applicable Creative Commons License

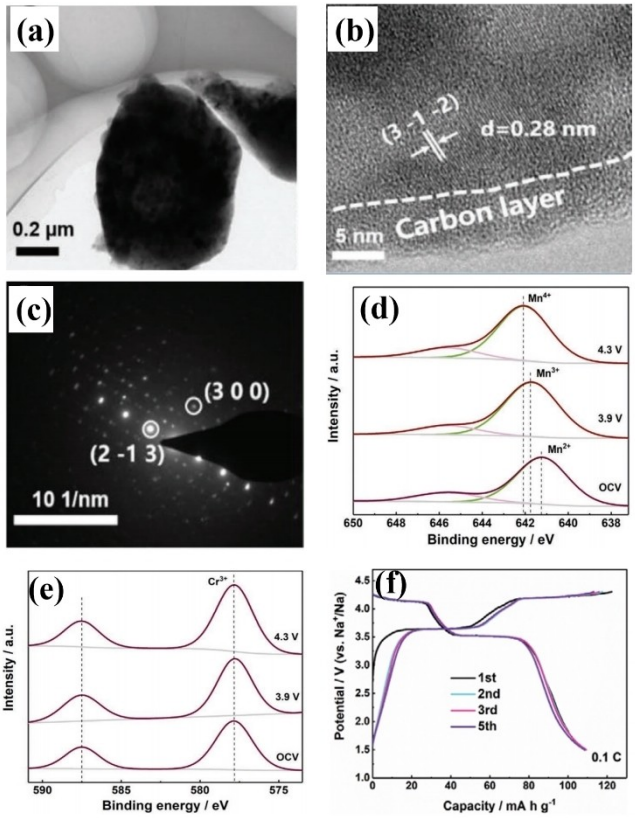

Figure 9. Characterizations of the as-prepared $Na_4MnCr(PO_4)_3$ material. (a) SEM images (b) the corresponding schematic structure of $Na_4MnCr(PO_4)_3$, (c) SAED pattern, (d, e) XPS spectra of Mn $2p_{3/2}$ and Cr 2p in the $Na_4MnCr(PO_4)_3$ under different charging states, respectively. (f) Charge/discharge curves at 0.1 C (1 C = 100 mA g^{-1}). (Reproduced from Ref. [79] Copyright (2020) with permission from Wiley.)

et al.[53] successfully induced the participation of 2.35 Na^+ in the electrochemical reaction, enhancing the reversibility of the redox at 3.59 V vs. Na^+/Na in $Na_4MnCr(PO_4)_3$, proving Mn^{2+}/Mn^{3+} and Mn^{3+}/Mn^{4+} active from Na4 to Na2 at voltages of 3.9 V and 4.3 V, and Cr^{3+}/Cr^{4+} from Na2 to Na1 near 4.3 V. However, structural transformation during charge and discharge cycles results in capacity fading when extracting the third Na ion.[81]

To address the instability of Mn-based NASICON structures, Hou et al.[82] introduced SiO_4 to replace PO_4, forming $Na_4MnCr(PO_4)_{2.9}(SiO_4)_{0.1}$ (NMCP-Si). This strategy, backed by both experimental and theoretical studies, uncovered how SiO_4 substitution refines electronic structures and Na storage properties. NMCP-Si showcased significantly improved rate capability and stability due to suppressed Jahn-Teller distortion of Mn^{3+} ions, enhancing Na ion diffusion and electrochemical kinetics. Table 6 presents the electrochemical performance of Mn-containing compounds as cathode materials for SIB, as outlined below.

The novel NASICON-type $Na_4MnCr(PO_4)_3$ material with high Na content delivers more specific discharge capacity because of three kinds of redox reactions. Super long cycles may benefit from the special storage sodium mechanism that involves two-phase transfer and solid-solution evolution during the shuttle of

Table 6. Electrochemical performance of Mn-based compounds

Mn-based compounds	Voltage (V)	Rate (C)	Capacity (mAh g^{-1})	Cycles
[77]$Na_3MnZr(PO_4)_3$,	4.0/3.5	10	105 (1.0 C, 2.5–4.7 V)	500
[80]$Na_4MnCr(PO_4)_3$	4.15/3.5	10	104.8 (0.1 C, 2.5–4.7 V)	500
[53]$Na_4MnCr(PO_4)_3$	4.35/ 4.0/3.5	5	130 (0.05 C, 1.5–4.5 V)	1000
[82]$Na_4MnCr(PO_4)_{2.9}(SiO_4)_{0.1}$	4.31/4.0	10	114.4 (0.1 C,1.5–4.3 V)	500

Na^+ ions, which helps lower the diffusion energy barrier due to the existence of the intermediate phase so as to stabilize the structure. Another reason is that the redox reactions of Mn^{2+}/Mn^{3+}, Mn^{3+}/Mn^{4+} and Cr^{3+}/Cr^{4+} occur at different voltage ranges and adopt different Na^+ diffusion paths. Fully activating the secondary redox of Mn^{4+}/Mn^{3+} can significantly boost the energy density of Mn-based polyanion-type compounds. However, structural degradation caused by Jahn-Teller distortions of Mn^{3+} remains challenging and degenerate, although introducing a transitional metal such as Zr, Cr into the Mn site can stabilize Mn-based structures and enhance Na^+ conductivity, perhaps by increasing other cation sites to enhance the structure. It is undeniable that the high electrochemical activity is attributed to the robust framework structure, minimal structural change and fast kinetics. There is still much research space regarding the sodium storage mechanism to explore more Na^+ ions to further increase the energy density while preserving the robust framework.

2.6. Fe-Based Redox

In the earlier stages of the study, the voltage plateau of the Fe^{2+}/Fe^{3+} redox couple within phosphates was notably low at around 2.5 V,[83] significantly limiting energy density. $NaFePO_4$ was recognized to exist in two distinct phases, olivine and maricite, with the latter previously deemed electrochemically inactive. However, in a groundbreaking study in 2014, Kim et al.[84] first reported the potential of the maricite-phase $NaFePO_4$ as an excellent cathode material, emphasizing the crucial role of its nano-sized form in facilitating the extraction of Na ions. Subsequently, researchers discovered a third amorphous phase,[85] which helps to buffer the significant lattice changes that occur between the pristine phase and the final phase, thereby reducing the transition stress and improving cycling stability. Fan et al.[19] revealed that the amorphous structure of $NaFePO_4$ served as a highly active cathode in sodium-ion batteries, with the high-energy ball-milling technique enhancing its specific capacities. Detailed structural characterizations revealed that the ordered maricite $NaFePO_4$ with

© 2024 Wiley-VCH GmbH

25666223, 2024, 12, Downloaded from https://chemistry-europe.onlinelibrary.wiley.com/doi/10.1002/batt.202400290 by University of Ulsan, Wiley Online Library on [11/11/2025]. See the Terms and Conditions (https://onlinelibrary.wiley.com/terms-and-conditions) on Wiley Online Library for rules of use; OA articles are governed by the applicable Creative Commons License

nano-sized (Figure 10a) and single-phase crystal embedded into amorphous matrix (figure 10b–c). This maricite/amorphous composite structure may enhance cycling stability by alleviating crack-induced capacity fading. For NFP-15, the Na K-edge XANE spectra demonstrated a similar peak with the maricite (Figure 10d), while the O K-edge XANE spectra showed that the peak related to Fe 3d has the highest intensity, indicating a decrease of the coordination number of O for NFP-15 compared to other types (Figure 10e), leading to the Fe localized environments from coplanar FeO_6 octahedra to FeO_n polyhedral (Figure 10f). This result is confirmed by the enhanced electrochemical performances, showing a discharge capacity over 105 mAh g^{-1} (Figure 10g) with 91.3% capacity retention (Figure 10g) even after 800 cycles at 1 C (Figure 10h). Besides, the excellent rate capability was provided as shown in Figure 10i (52 mAh g^{-1} even at 10 C). Additionally, further activation of the Fe^{3+}/Fe^{4+} redox couple is expected in $Na_3Fe_2(PO_4)_3$. Rajagopalan et al.[86] explored the Fe^{4+}/Fe^{3+} reversible redox behavior in $Na_3Fe_2(PO_4)_3$/C wrapped with conducting carbon network, showing a notable voltage plateau at about 3.4 V, a superior discharge capacity of 109 mAh g^{-1} with no capacity fading after 200 cycles, showcasing an advancement over other iron-based polyanion structures owing to its flexible 3D open framework.

Furthermore, recent research has redirected attention towards the mixed anion-group compound $Na_4Fe_3(PO_4)_2P_2O_7$, owing to its remarkable electrochemical performance, primarily attributed to the extraction of three Na^+ ions. Kang et al.[78]

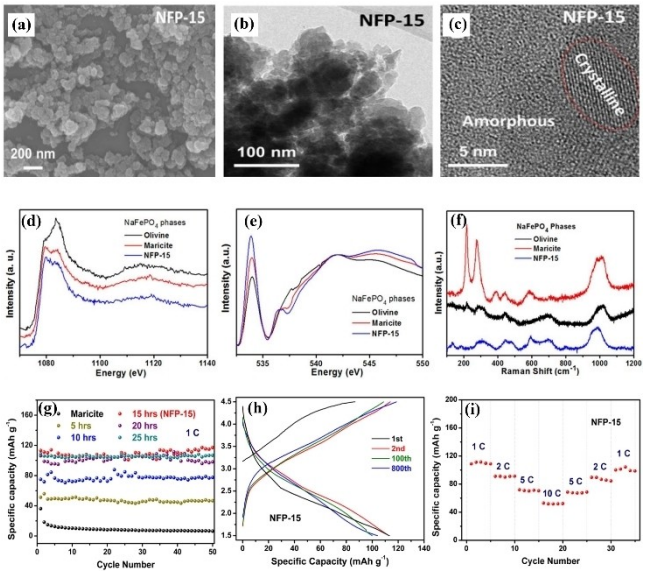

Figure 10. Structure and morphology of polymorphic composites. polymorphic composites obtained by milling at 600 rpm for 15 hours (NFP-15) (a) SEM image, (b) TEM image, (c) HRTEM image. X-ray absorption near edge structure spectra of (d) Na K-edge, (e) O K-edge for olivine-type, (f) Raman spectra of maricite-type, olivine-type and NFP-15. Electrochemical performances of electrode, (g) Cycling stability at 1 C (1 C = 155 mA g^{-1}) of the polymorphic composites obtained by milling at 600 rpm for 5, 10, 15, 20, and 25 hours, together with the as-prepared maricite $NaFePO_4$, (h) The charge/discharge curves at 1 C of the NFP-15, (i) The rate performance of NFP-15 in the range of 1.5 and 4.5 V, sodium pellet as the anode, and $NaPF_6$ with 1 mol L^{-1} dissolved in an equal volume ratio EC-PC solution as the electrolyte. (Reproduced from Ref. [19] Copyright (2019) with permission from Elsevier)

reported that this compound, based on the Fe^{2+}/Fe^{3+} redox pair, achieves a capacity of up to 129 mAh g^{-1} at 3.2 V, surpassing the performance of the earlier iron-based phosphates or pyrophosphates. Within its crystal structure, there are four distinguishable Na sites with varying oxygen coordination, organized within a three-dimensional framework in bc plane-parallel $[Fe_3P_2O_{13}]\infty$ layers connected by $[P_2O_7]$ groups on the a-axis. This unique arrangement enhances high ionic conductivity, facilitating Na^+ transfer between layers and outperforming the conductivity of the maricite-$NaFePO_4$, Na_2FePO_4F,[87,25] and pyrophosphate $Na_2FeP_2O_7$.[24] Chou et al.[88] have further confirmed the compound's minimal volumetric change, demonstrating cycling over more than 4400 iterations and its stability in air, contrasting with the air vulnerability of pyrophosphates. The sodium ion diffusion coefficients were highly comparable to similar orders of magnitude of known NASICON-type cathode materials, and four redox peaks were identified within a voltage window of 2.7–4.1 V. However, $Na_4Fe_3(PO_4)_2P_2O_7$ has been underestimated because pure-phase material is difficult to obtain due to the presence of a minor $NaFePO_4$ impurity.[84] Significant improvements have been made by Du et al.[89] They made substantial advancements by synthesizing the pure-phase non-stoichiometric compound $Na_{3.4}Fe_{2.4}(PO_4)_{1.4}P_2O_7$ through a solid-solution approach. The process of removing impurities enhanced sodium ion diffusion, allowing the compound to achieve superior stability over 14000 cycles. Furthermore, the different phenomenon observed in the charge-discharge profile indicates a different process from $LiFePO_4$, with capacity loss attributed to the inability of Na^+ ions to re-enter the pristine phase during discharge. The purity of the synthesized phase plays a crucial role in ensuring better performance even with a high loading mass of 40 mg cm^{-2}, suggesting the significance of the storage process in achieving good performance.

Exploring iron-based sulfates for high Fe^{2+}/Fe^{3+} redox potential, experiments have shown promise in sodium variants like $Na_2Fe(SO_4)_2$, which produce an average voltage of 3.4 V and yield a modest capacity of about 70 mAh/g.[29] In contrast, $Na_2Fe_2(SO_4)_3$ with alluaudite polymorph exhibits highly electrochemical activity, benefiting from an easier ion diffusion route, connecting Fe_2O_{10} dimers with SO_4 tetrahedra into an open lattice structure. Therefore, $Na_2Fe_2(SO_4)_3$ as a cathode material for SIB theoretically could achieve a reversible capacity exceeding 100 mAh g^{-1} and a voltage output around 3.8 V. However, off-stoichiometric compounds like $Na_{2+2x}Fe_{2-x}(SO_4)_3$ are often obtained, and their electrochemical performance is not positive, possibly due to the intrinsic structural defects from moisture absorption.[90] Minkyu Kim et al.[91] designed a novel triplite-type iron fluoro-sulfate $NaFeSO_4F$ with disordered cation arrangement, enabling shrinkage of the crystal volume despite facing significant distortion. Unfortunately, the structure can only be obtained through a solid-state reaction, which requires high activation energy. This compound achieves a practical energy density (~430 Wh kg^{-1}) on par with several Li-ion battery cathodes like $LiMn_2O_4$ (430 Wh kg^{-1}). Na_2FeSiO_4 has emerged as an efficient option owing to its high theoretical capacity of roughly 276 mAh g^{-1}.[17] Kee et al.[92] successfully synthesized this material using a solvothermal method for SIB cathode

© 2024 Wiley-VCH GmbH

25666223, 2024, 12, Downloaded from https://chemistry-europe.onlinelibrary.wiley.com/doi/10.1002/batt.202400290 by University of Ulsan, Wiley Online Library on [11/11/2025]. See the Terms and Conditions (https://onlinelibrary.wiley.com/terms-and-conditions) on Wiley Online Library for rules of use; OA articles are governed by the applicable Creative Commons License

application, achieving a noteworthy initial capacity of roughly 126 mAh g^{-1}. The electrochemical performance of Fe-containing compounds is compiled in Table 7.

Currently, the mixed-anion-group Fe-based phosphate material $Na_4Fe_3(PO_4)_2P_2O_7$ has the most favorable cycling stability and highest rate performance. The challenge lies in obtaining a high-purity phase due to the complex and mixed anions during the synthesis process, ultimately resulting in the formation of a layered structure comprising alternating PO_4-P_2O_7 layers connected by corners. The unique configuration facilitates rapid and stable Na^+ transportation, resulting in high ionic conductivity. Additionally, the high electrochemical performance relies on material purity. However, $Na_4Fe_3(PO_4)_2P_2O_7$ is excluded due to its low energy density, its modest working potential of around 3.0 V, and the presence of large anionic groups. Iron-based materials, abundant and non-toxic, hold promise for future large-scale production. Particularly noteworthy is $Na_2Fe_2(SO_4)_3$, offering a 3.8 V operating voltage versus sodium based on the Fe^{2+}/Fe^{3+} redox couple, reflecting the highest redox potential among materials.

For sodium-ion batteries, high-voltage systems ideally utilize resourceful, inexpensive and environmental friendly materials such as Fe, Cr and Mn as redox centers. NASICON structure phosphate compounds, known for their high thermal stability, have shown significant improvements in energy density, cycling stability and rate performance. These enhancements correlate with improved electronic conductivity and reduced charge transfer impedance due to the dual functions of carbon coating and ion doping. However, their low energy density limits practical application when assembling into a full cell using hard carbon as anode, as the Na-metal faces complex challenges in safety and interfacial stability. Nanostructure may alleviate these limitations, although they present challenges in production lines and potential cost escalation. Pyrophosphate-based cathode materials still suffer from low energy density due to the large groups $P_2O_7^{4-}$, along with thermodynamic issues. Mixed phosphate and pyrophosphate encounter similar issues. Compounds composed of smaller anionic group with strong electronegative such as SO_4^{2-}, SiO_4^{-}, and F^{-}, or their combinations, exhibit high operation voltage; however, they suffer from unstable cycling stability, susceptibility to hydrolyze in air, and difficulty in obtaining material purity. Consequently, NASICON structure materials, combined with cost-effective, abundant, and non-toxic metal redox to form polyanionic type cathodes for SIBs, present a preferable choice.

Table 7. Electrochemical performance of Fe-based compounds.

Fe-based compounds	Voltage (V)	Rate (C)	Capacity (mAh g^{-1})	Cycles
[78] $Na_4Fe_3(PO_4)_2P_2O_7$	3.2	20	129 (0.05 C, 2.7–4.1 V)	1000
[88] $Na_4Fe_3(PO_4)_2P_2O_7$/C	3.2	20	113 (0.05 C, 2.7–4.1 V)	4400
[89] $Na_{3.4}Fe_{2.4}(PO_4)_{1.4}P_2O_7$	2.88 3.18	100	110.8 (0.1 C,1.5-4.1 V)	14000
[29] $Na_2Fe(SO_4)_2$	3.6	2	82 (0.1 C,1.5–4.1 V)	100
[91] $NaFeSO_4F$	3.7	1	138 (0.01 C, 2.5–4.1 V)	50
[92] Na_2FeSiO_4	No obvious plateau	0.05	126 (0.025 C,1.0–4.1 V)	5

3. Summary and Outlook

In this review, we provide an overview of recent advances in high voltage polyanionic cathode materials based on metal redox couples. When considering their commercial viability, factors such as operation voltage, energy density, cost, and environmental friendliness come to the forefront. Consequently, cathode materials containing Co, Ni, Cr, and V were excluded due to cost considerations, toxicity concerns, and cycling instability issues associated with the current electrolyte. Instead, cathode materials incorporating Fe and Mn may present a better choice due to their cost-effectiveness and abundance. Various strategies, such as elemental doping, surface coating with protective layers, special structure and composition design, have shown potential in enhancing the performance of these materials. In fact, the success of Fe-based lithium-ion batteries underscores this point. Moreover, another advantage of thermal stability also remains crucial, particularly in energy storage system applications, which are the target market of SIBs. Additionally, the low mass and volume energy density of Fe and Mn-based cathode batteries may be less crucial for stationary applications, but it is still meaningful to reduce the total cost of SIBs. Therefore, significant challenges persist in the development of full-cell SIBs, particularly in cathode development. We anticipate that sustained efforts in research and development will drive the advancement of polyanion-type materials and foster their practical application.

Acknowledgements

This work was supported by the Doctoral Foundation of Taiyuan Institute of Technology (2022KJ054) and Shanxi Key Laboratory of Biomass-based Green Methanol Conversion and Hydrogen Utilization. We would also like to thank the researchers for their assistance with revisions and expert suggestions.

Conflict of Interests

The authors declare no conflict of interest.

Keywords: doping · electrochemistry · polyanions · sodium · synthesis design

© 2024 Wiley-VCH GmbH

25666223, 2024, 12, Downloaded from https://chemistry-europe.onlinelibrary.wiley.com/doi/10.1002/batt.202400290 by University of Ulsan, Wiley Online Library on [11/11/2025]. See the Terms and Conditions (https://onlinelibrary.wiley.com/terms-and-conditions) on Wiley Online Library for rules of use; OA articles are governed by the applicable Creative Commons License

[1] Y. You, H. Yao, S. Xin, Y. Yin, T. Zuo, C. Yang, Y. Guo, Y. Cui, L. Wan, J. B. Goodenough, *Adv. Mater.* **2016**, *28*, 7243.
[2] Y. Fang, L. Xiao, X. Ai, Y. Cao, H. Yang, *Adv. Mater.* **2015**, *27*, 5895.
[3] D. Kundu, E. Talaie, V. Duffort, L. F. Nazar, *Angew. Chem. Int. Ed.* **2015**, *54*, 3431.
[4] H. S. Hirsh, Y. Li, D. H. S. Tan, M. Zhang, E. Zhao, Y. S. Meng, *Adv. Energy Mater.* **2020**, *10*, 2001274.
[5] K. Kubota, I. Ikeuchi, T. Nakayama, C. Takei, N. Yabuuchi, H. Shiiba, M. Nakayama, S. Komaba, *J. Phys. Chem. C* **2015**, *119*, 166.
[6] M. Keller, D. Buchholz, S. Passerini, *Adv. Energy Mater.* **2016**, *6*, 1501555.
[7] P. Wang, Y. You, Y. Yin, Y. Guo, *Adv. Energy Mater.* **2018**, *8*, 1701912.
[8] T. Cui, L. Liu, Y. Xiang, C. Sheng, X. Li, Y. Fu, *J. Am. Chem. Soc.* **2024**, *146*, 13924.
[9] Q. Ni, Y. Bai, F. Wu, C. Wu, *Adv. Sci.* **2017**, *4*, 1600275.
[10] H. Li, M. Xu, Z. Zhang, Y. Lai, J. Ma, *Adv. Funct. Mater.* **2020**, *30*, 2000473.
[11] T. Jin, Q. Han, L. Jiao, *Adv. Mater.* **2020**, *32*, 1806304.
[12] C. Cai, Q. Liu, Z. Hu, S. Chen, W. Zhang, Z. Wang, J. Liu, C. Fan, *J. Power Sources* **2023**, *571*, 233080.
[13] X. Liu, L. Tang, Z. Li, J. Zhang, Q. Xu, H. Liu, Y. Wang, Y. Xia, Y. Cao, X. Ai, *J. Mater. Chem. A* **2019**, *7*, 18940.
[14] W. Song, X. Ji, Y. Zhu, H. Zhu, F. Li, J. Chen, F. Lu, Y. Yao, Craig. E. Banks, *ChemElectroChem* **2014**, *1*, 871.
[15] P. Hu, X. Wang, T. Wang, L. Chen, J. Ma, Q. Kong, S. Shi, G. Cui, *Adv. Sci.* **2017**, *4*, advs.201600525.
[16] H. Kim, C. S. Park, J. W. Choi, Y. Jung, *Angew. Chem. Int. Ed.* **2016**, *55*, 6662.
[17] T. Jin, H. Li, K. Zhu, P.-F. Wang, P. Liu, L. Jiao, *Chem. Soc. Rev.* **2020**, *49*, 2342.
[18] M. Avdeev, Z. Mohamed, C. D. Ling, J. Lu, M. Tamaru, A. Yamada, P. Barpanda, *Inorg. Chem.* **2013**, *52*, 8685.
[19] F. Xiong, Q. An, L. Xia, Y. Zhao, L. Mai, H. Tao, Y. Yue, *Nano Energy* **2019**, *57*, 608.
[20] B. Wu, G. Hou, E. Kovalska, V. Mazanek, P. Marvan, L. Liao, L. Dekanovsky, D. Sedmidubsky, I. Marek, C. Hervoches, Z. Sofer, *Inorg. Chem.* **2022**, *61*, 4092.
[21] F. Bianchini, H. Fjellvåg, P. Vajeeston, *Mater. Chem. Phys.* **2018**, *219*, 212.
[22] A. K. Padhi, K. S. Nanjundaswamy, C. Masquelier, S. Okada, J. B. Goodenough, *J. Electrochem. Soc.* **1997**, *144*, 1609.
[23] K. Kawai, W. Zhao, S. Nishimura, A. Yamada, *ACS Appl. Energ. Mater.* **2018**, *1*, 928.
[24] P. Barpanda, G. Liu, C. D. Ling, M. Tamaru, M. Avdeev, S.-C. Chung, Y. Yamada, A. Yamada, *Chem. Mater.* **2013**, *25*, 3480.
[25] Q. Li, Z. Liu, F. Zheng, R. Liu, J. Lee, G. Xu, G. Zhong, X. Hou, R. Fu, Z. Chen, K. Amine, J. Mi, S. Wu, C. P. Grey, Y. Yang, *Angew. Chem. Int. Ed.* **2018**, *57*, 11918.
[26] M. Law, V. Ramar, P. Balaya, *J. Power Sources* **2017**, *359*, 277.
[27] K. Kaliyappan, Z. Chen, *Electrochim. Acta* **2018**, *283*, 1384.
[28] J. C. Treacher, S. M. Wood, M. S. Islam, E. Kendrick, *Phys. Chem. Chem. Phys.* **2016**, *18*, 32744.
[29] W. Pan, W. Guan, S. Liu, B. B. Xu, C. Liang, H. Pan, M. Yan, Y. Jiang, *J. Mater. Chem. A* **2019**, *7*, 13197.
[30] A. Yamada, *Molecules* **2021**, *26*, 5143.
[31] Y. You, A. Manthiram, *Adv. Energy Mater.* **2018**, *8*, 1701785.
[32] A. Gutierrez, N. A. Benedek, A. Manthiram, *Chem. Mater.* **2013**, *25*, 4010.
[33] X. Zhong, Z. Yang, Y. Jiang, W. Li, L. Gu, Y. Yu, *ACS Appl. Mater. Interfaces* **2016**, *8*, 32360.
[34] W. Zhou, L. Xue, X. Lü, H. Gao, Y. Li, S. Xin, G. Fu, Z. Cui, Y. Zhu, J. B. Goodenough, *Nano Lett.* **2016**, *16*, 7836.
[35] C. Zhang, D. Guo, J. Qin, B. Mao, M. Cao, *Mater. Lett.* **2017**, *195*, 205.
[36] Y. Chen, J. Cheng, Y. Wang, C. Wang, Z. He, D. Li, L. Guo, *J. Mater. Sci.* **2020**, *55*, 13141.
[37] X. Liu, G. Feng, E. Wang, H. Chen, Z. Wu, W. Xiang, Y. Zhong, Y. Chen, X. Guo, B. Zhong, *ACS Appl. Mater. Interfaces* **2019**, *11*, 12421.
[38] S. K. Pal, R. Thirupathi, S. Chakrabarty, S. Omar, *ACS Appl. Energ. Mater.* **2020**, *3*, 12054.
[39] T. I. Perfilyeva, A. M. Alekseeva, O. A. Drozhzhin, E. V. Antipov, *Russ. J. Electrochem.* **2023**, *59*, 481.
[40] B. Li, J. Mei, X. Wang, C. Shang, X. Shen, P. Hu, *Energy Fuels* **2024**, *38*, 1508.
[41] M. Chen, W. Hua, J. Xiao, J. Zhang, V. W. Lau, M. Park, G.-H. Lee, S. Lee, W. Wang, J. Peng, L. Fang, L. Zhou, C.-K. Chang, Y. Yamauchi, S. Chou, Y.-M. Kang, *J. Am. Chem. Soc.* **2021**, *143*, 18091.
[42] Y. Chen, Y. Xu, X. Sun, B. Zhang, S. He, C. Wang, *J. Power Sources* **2018**, *397*, 307.
[43] J. Kim, I. Park, H. Kim, K. Park, Y. Park, K. Kang, *Adv. Energy Mater.* **2016**, *6*, 1502147.
[44] S. Y. Lim, H. Kim, J. Chung, J. H. Lee, B. G. Kim, J.-J. Choi, K. Y. Chung, W. Cho, S.-J. Kim, W. A. Goddard, Y. Jung, J. W. Choi, *Proc. Nat. Acad. Sci.* **2014**, *111*, 599.
[45] W. Fang, Z. An, J. Xu, H. Zhao, J. Zhang, *RSC Adv.* **2018**, *8*, 21224.
[46] V. M. Kovrugin, J.-N. Chotard, F. Fauth, A. Jamali, R. David, C. Masquelier, *J. Mater. Chem. A* **2017**, *5*, 14365.
[47] M. J. Aragón, P. Lavela, R. Alcántara, J. L. Tirado, *Electrochim. Acta* **2015**, *180*, 824.
[48] J. Wang, X. Lai, Z.-X. Li, P. Wang, J.-H. Zhang, T.-F. Yi, *J. Ind. Eng. Chem.* **2024**, S1226086X24000479.
[49] G. Hautier, A. Jain, S. P. Ong, B. Kang, C. Moore, R. Doe, G. Ceder, *Chem. Mater.* **2011**, *23*, 3495.
[50] M. Herklotz, F. Scheiba, R. Glaum, E. Mosymow, S. Oswald, J. Eckert, H. Ehrenberg, *Electrochim. Acta* **2014**, *139*, 356.
[51] K. Kawai, D. Asakura, S. Nishimura, A. Yamada, *Chem. Commun.* **2019**, *55*, 13717.
[52] J. Zhang, G. Liang, C. Wang, C. Lin, J. Chen, Z. Zhang, X. S. Zhao, *ACS Appl. Mater. Interfaces* **2020**, *12*, 28313.
[53] J. Wang, Y. Wang, D. Seo, T. Shi, S. Chen, Y. Tian, H. Kim, G. Ceder, *Adv. Energy Mater.* **2020**, *10*, 1903968.
[54] J. Zhang, Y. Liu, X. Zhao, L. He, H. Liu, Y. Song, S. Sun, Q. Li, X. Xing, J. Chen, *Adv. Mater.* **2020**, *32*, 1906348.
[55] K. Kawai, D. Asakura, S. Nishimura, A. Yamada, *Chem. Mater.* **2021**, *33*, 1373.
[56] J. Zhang, G. Liang, C. Wang, C. Lin, J. Chen, Z. Zhang, X. S. Zhao, *ACS Appl. Mater. Interfaces* **2020**, *12*, 28313.
[57] A. Gutierrez, S. Kim, T. T. Fister, C. S. Johnson, *ACS Appl. Mater. Interfaces* **2017**, *9*, 4391.
[58] A. Chiring, M. Mazumder, S. K. Pati, C. S. Johnson, P. Senguttuvan, *J. Solid State Chem.* **2021**, *293*, 121766.
[59] H. Kim, C. S. Park, J. W. Choi, Y. Jung, *Chem. Mater.* **2016**, *28*, 6724.
[60] H. Kim, C. S. Park, J. W. Choi, Y. Jung, *Angew. Chem.* **2016**, *128*, 6774.
[61] M. Nose, H. Nakayama, K. Nobuhara, H. Yamaguchi, S. Nakanishi, H. Iba, *J. Power Sources* **2013**, *234*, 175.
[62] M. Zarrabeitia, M. Jáuregui, N. Sharma, J. C. Pramudita, M. Casas-Cabanas, *Chem. Mater.* **2019**, *31*, 5152.
[63] H. Zhang, I. Hasa, D. Buchholz, B. Qin, D. Geiger, S. Jeong, U. Kaiser, S. Passerini, *NPG Asia Mater.* **2017**, *9*, e370.
[64] J. Zeng, D. Guan, W. Wang, X. Tan, Y. Cao, Z. Peng, G. Hu, K. Du, *ACS Appl. Energ. Mater.* **2023**, *6*, 4238.
[65] X. Cao, Y. Xu, L. Zhang, M. H. Engelhard, L. Zhong, X. Ren, H. Jia, B. Liu, C. Niu, B. E. Matthews, H. Wu, B. W. Arey, C. Wang, J.-G. Zhang, W. Xu, *ACS Energy Lett.* **2019**, *4*, 2529.
[66] A. Chari, K. El Ouardi, M. Tayoury, M. Aqil, B. Orayech, A. El Bouari, J. Alami, M. Dahbi, *J. Power Sources* **2022**, *548*, 232046.
[67] K. Kubota, K. Yokoh, N. Yabuuchi, S. Komaba, *Electrochemistry* **2014**, *82*, 909.
[68] L. Tang, X. Liu, Z. Li, X. Pu, J. Zhang, Q. Xu, H. Liu, Y.-G. Wang, Y. Xia, *ACS Appl. Mater. Interfaces* **2019**, *11*, 27813.
[69] M. Zarrabeitia, M. Jáuregui, N. Sharma, J. C. Pramudita, M. Casas-Cabanas, *Chem. Mater.* **2019**, *31*, 5152.
[70] A. Chari, K. El Ouardi, M. Tayoury, M. Aqil, B. Orayech, A. El Bouari, J. Alami, M. Dahbi, *J. Power Sources* **2022**, *548*, 232046.
[71] S. P. Ong, V. L. Chevrier, G. Hautier, A. Jain, C. Moore, S. Kim, X. Ma, G. Ceder, *Energy Environ. Sci.* **2011**, *4*, 3680.
[72] P. R. Kumar, H. B. Yahia, I. Belharouak, M. T. Sougrati, S. Passerini, R. Amin, R. Essehli, *J. Solid State Electrochem.* **2020**, *24*, 17.
[73] D. Kundu, R. Tripathi, G. Popov, W. R. M. Makahnouk, L. F. Nazar, *Chem. Mater.* **2015**, *27*, 885.
[74] V. Priyanka, G. Savithiri, R. Subadevi, M. Sivakumar, *Appl. Nanosci.* **2020**, *10*, 3945.
[75] V. Priyanka, G. Savithiri, P. Rajkumar, T. Meenatchi, R. Subadevi, M. Sivakumar, *J. Solid State Chem.* **2020**, *290*, 121551.
[76] H. Gao, Y. Li, K. Park, J. B. Goodenough, *Chem. Mater.* **2016**, *28*, 6553.
[77] H. Gao, I. D. Seymour, S. Xin, L. Xue, G. Henkelman, J. B. Goodenough, *J. Am. Chem. Soc.* **2018**, *140*, 18192.
[78] H. Kim, G. Yoon, I. Park, J. Hong, K.-Y. Park, J. Kim, K.-S. Lee, N.-E. Sung, S. Lee, K. Kang, *Chem. Mater.* **2016**, *28*, 7241.
[79] A. Mullaliu, M. Gaboardi, J. R. Plaisier, S. Passerini, M. Giorgetti, *ACS Appl. Energ. Mater.* **2020**, *3*, 5728.
[80] W. Zhang, H. Li, Z. Zhang, M. Xu, Y. Lai, S. Chou, *Small* **2020**, *16*, 2001524.

© 2024 Wiley-VCH GmbH

25666223, 2024, 12, Downloaded from https://chemistry-europe.onlinelibrary.wiley.com/doi/10.1002/batt.202400290 by University of Ulsan, Wiley Online Library on [11/11/2025]. See the Terms and Conditions (https://onlinelibrary.wiley.com/terms-and-conditions) on Wiley Online Library for rules of use; OA articles are governed by the applicable Creative Commons License

[81] F. Chen, V. M. Kovrugin, R. David, O. Mentré, F. Fauth, J. Chotard, C. Masquelier, *Small Methods* **2019**, *3*, 1800218.
[82] Y. Hou, Q. Liu, L. Yang, J. Hu, Z. Wang, X. Zhang, J. Pan, Z. Bai, H. Wang, Z. Lu, *Small* **2023**, *19*, 2207466.
[83] C. Xu, J. Zhao, C. Yang, Y.-S. Hu, *ACS Cent. Sci.* **2023**, *9*, 1721.
[84] J. Kim, D.-H. Seo, H. Kim, I. Park, J.-K. Yoo, S.-K. Jung, Y.-U. Park, W. A. Goddard Iii, K. Kang, *Energy Environ. Sci.* **2015**, *8*, 540.
[85] K. Xiang, W. Xing, D. B. Ravnsbæk, L. Hong, M. Tang, Z. Li, K. M. Wiaderek, O. J. Borkiewicz, K. W. Chapman, P. J. Chupas, Y.-M. Chiang, *Nano Lett.* **2017**, *17*, 1696.
[86] R. Rajagopalan, B. Chen, Z. Zhang, X. Wu, Y. Du, Y. Huang, B. Li, Y. Zong, J. Wang, G. Nam, M. Sindoro, S. X. Dou, H. K. Liu, H. Zhang, *Adv. Mater.* **2017**, *29*, 1605694.
[87] B. L. Ellis, W. R. M. Makahnouk, Y. Makimura, K. Toghill, L. F. Nazar, *Nat. Mater.* **2007**, *6*, 749.
[88] M. Chen, W. Hua, J. Xiao, D. Cortie, W. Chen, E. Wang, Z. Hu, Q. Gu, X. Wang, S. Indris, S.-L. Chou, S.-X. Dou, *Nat. Commun.* **2019**, *10*, 1480.
[89] Z. Fan, W. Song, N. Yang, C. Lou, R. Tian, W. Hua, M. Tang, F. Du, *Angew. Chem.* **2024**, e202316957.
[90] Y. Liu, R. Rajagopalan, E. Wang, M. Chen, W. Hua, B. Zhong, Y. Zhong, Z. Wu, X. Guo, *ACS Sustainable Chem. Eng.* **2018**, *6*, 16105.
[91] M. Kim, D. Kim, W. Lee, H. M. Jang, B. Kang, *Chem. Mater.* **2018**, *30*, 6346.
[92] Y. Kee, N. Dimov, A. Staykov, S. Okada, *Mater. Chem. Phys.* **2016**, *171*, 45.

Manuscript received: April 29, 2024
Revised manuscript received: June 17, 2024
Accepted manuscript online: June 28, 2024
Version of record online: August 20, 2024

© 2024 Wiley-VCH GmbH

25666223, 2024, 12, Downloaded from https://chemistry-europe.onlinelibrary.wiley.com/doi/10.1002/batt.202400290 by University of Ulsan, Wiley Online Library on [11/11/2025]. See the Terms and Conditions (https://onlinelibrary.wiley.com/terms-and-conditions) on Wiley Online Library for rules of use; OA articles are governed by the applicable Creative Commons License